Universidade Federal de Ouro Preto
Departamento de Engenharia Civil
Programa de Pós Graduação em Engenharia Civil
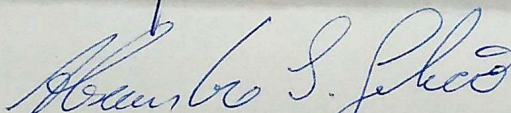
THE INFLUENCE OF GEOMETRICALLY NONLINEAR EFFECTS ON THE PROGRESSIVE COLLAPSE OF REINFORCED CONCRETE STRUCTURES

Cláudio Ernani Martins Oliveira

Thesis carried out under the supervision of the Federal University of Ouro Preto (UFOP) and presented as a requirement for obtaining the degree of Doctor of Philosophy in Engineering Sciences.

Advisor: Ricardo A. da Mota Silveira

Ouro Preto

February, 2015

THE INFLUENCE OF GEOMETRICALLY NONLINEAR EFFECTS ON THE PROGRESSIVE COLLAPSE OF REINFORCED CONCRETE STRUCTURES

AUTOR: CLÁUDIO ERNANI MARTINS OLIVEIRA

Esta tese foi apresentada em sessão pública e aprovada em 26 de fevereiro de 2015, pela Banca Examinadora composta pelos seguintes membros:

Prof. Ricardo Azoubel da Mota Silveira, D.Sc.– UFOP (Presidente)

Prof. Alexandre da Silva Galvão, D.Sc. – UFSJ

Prof. Francisco Célio de Araújo, D.Ing. – UFOP

Prof. João Batista Marques de Sousa Jr.– UFC

Prof. Walnório Graça Ferreira, D.Sc. – UFES

Never say someone is a coward
for giving up... it takes incredible
courage to admit defeat.
(myself *)*

Acknowledgements

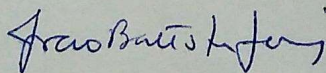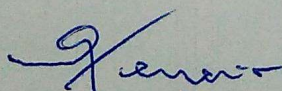To my advisor, Prof. Ricardo Silveira, without whom this work would not be possible;

To Prof. Thierry Massart and Dr. Peter Berke, for their undeniable commitment and professionalism;

To Prof. Philippe Bouillard, for giving me a chance to prove myself;

To Rodrigo, for being a great partner and, now, husband;

To my family, just because;

To the friends I had and specially to the ones I still have after these 5 long years of 'I'm not in the mood', 'maybe another time' and 'I'm kinda sick';

To my co-workers at Propec, because they know what it is like and to the wonderful people I met at BATir (sometimes, the world should be a little smaller); Special thanks to Everton and Adrian for helping with the models;

To Eliana, who sometimes believes me more than I do;

To the staff at UFOP and ULB, those who keep the wheels turning;

To UNIFEI, for allowing me 10 hours of participation in a post-graduation program since February/2014;

To CAPES, for the financial support and for granting me the PDSE scholarship (process 9533/12-5);

To the agencies that support research in Brazil (CAPES, CNPq, FAPEMIG, *etc.*).

Abstract

A multilayered Bernoulli beam finite element, including elasto-plastic material behavior of the constituents within a corotational, geometrically nonlinear framework is applied to investigate the behavior of reinforced concrete structures. The investigation aims at the propagation of the damage induced by the loss of a column and verifies whether or not the process of progressive collapse is initiated. For the analysis, the material nonlinearity is represented using unidimensional constitutive laws in the material layers. The multilayered discretization on the sectional level allows describing the gradual crushing of concrete, as well as the yielding and breaking of the reinforcement bars. The behavior of four planar frames is investigated computationally in this work. The first structure is a intermediate moment frame (IMF), while the second one is composed of a three-storey scale model (TSM), both representing parts of two different buildings in a quasi-static scenario. Computational results are compared to available experimental data from the literature both in terms of structural response (load *vs.* displacements curves) and failure mechanisms. Catenary effects are shown to play an important role in the structural behavior and to contribute to an increase of the load-bearing capacity of the damaged structure. A computational parametric study is also reported in order to assess how the physical parameters affect the overall structural behavior and to identify the main physical parameters affecting the studied problems. The third and fourth structures are five-storey planar frames, each realistically designed in accordance with the minimum requirements proposed by the reinforced concrete design/building codes of Europe and Brazil. Nonlinear dynamic analysis is performed, including elasto-viscoplastic effects. The load combinations considered for progressive collapse analysis follow the prescriptions of the Department of Defense of the United States. The work verifies if the minimum requirements of the considered codes are sufficient for enforcing structural safety and robustness, and also points out the major differences in terms of progressive collapse potential of the corresponding designed structures.

KEYWORDS: progressive collapse, reinforced concrete, nonlinear analysis, corotational formulation, multilayer discretization

Resumo

Este trabalho apresenta um elemento finito baseado na teoria de Bernoulli com seção transversal discretizada em camadas, associando elastoplasticidade e não linearidade geométrica em uma formulação corrotacional. A investigação proposta foca na propagação do dano induzido pela perda de um pilar e verifica se o processo de colapso progressivo é ou não iniciado. Nesta análise, a não linearidade física nas camadas da seção transversal é representada utilizando leis constitutivas unidimensionais. A discretização em camadas permite descrever o esmagamento gradual do concreto, assim como a plastificação e ruptura das barras de armadura. O comportamento de quato pórticos planos é investigado computacionalmente. Os dois primeiros (IMF e TSM, abreviaturas para *intermediate moment frame* e *three-storey scale model*) representam partes de edifícios em um cenário quase-estático. Resultados computacionais são comparados com dados experimentais disponíveis na literatura em termos de resposta estrutural (curvas carga *vs.* deslocamento) e mecanismos de falha. Os resultados mostram que os efeitos catenários afetam significativamente o comportamento estrutural e contribuem para um aumento da capacidade suporte da estrutura danificada. Um estudo paramétrico computacional é desenvolvido com a finalidade de entender como as propriedades dos materiais afetam o comportamento global das estruturas e identificar quais destas propriedades tem influência crucial nos cenários investigados. A terceira e quarta estruturas são pórticos planos de cinco andares, cada um idealizado de acordo com as normas de projeto/construção em concreto armado em vigor na Europa e no Brasil. Uma análise dinâmica não linear é desenvolvida. A combinação de cargas considerada para a análise de colapso progressivo segue as prescrições do Departamento de Defesa dos Estados Unidos. O trabalho verifica se as prescrições mínimas das normas de concreto armado utilizadas são suficientes para garantir segurança e robustez estrutural, além disso, aponta as diferenças em termos de propensão ao colapso progressivo.

PALAVRAS CHAVE: colapso progressivo, concreto armado, análise não linear, formulação corrotacional, discretização em camadas

Contents

List of Figures

List of Tables

Abbreviations

The following list of abbreviations is presented in alphabetical order:

3D	three-dimensional
2D	two-dimensional
ACI	American Concrete Institute
APM	Alternate Paht Method
ASCE	American Society of Civil Engineers
ASTM	American Society for Testing and Materials
BRCO	Brazilian model - corotational analysis
C_	class of concrete
CA_	class of steel
CC_	Consequence Class
CEN	Comité Européen de Normalisation
COMURBA	Companhia de Melhoramentos Urbanos
CPU	central processing unit
DoD	Department of Defense
ELRM	Enhanced Local Resistance Method
ELU	Estados Limite Últimos
EUCO	European model - corotational analysis
FEMA	Federal Emergency Management Agency
GEOM	geometrically
GSA	General Service Administration
HBR_	class of steel
ICC	International Code Council
IMF	Intermediate Moment Frame
ISC	Interagency Security Committee
MCFT	Modified Compression Field Theory
NBR	Norma Brasileira
NIST	National Institute of Standards ans Technology
NPS	National Park Service

NUM, num	numerical
PC	progressive collapse
PH	plastic hinge
PHM	Plastic Hinge Method
RC	reinforced concrete
S_	class of steel
SLRM	Specific Local Resistance Method
TFM	Tie Force Method
TSM	Three-story Scale Model
USA	United States of America
WTC	World Trade Center
c	compressive
conc	concrete
cor	corotational/corotated
cte.	constant
et al.	*et alii*
etc.	*et cetera*
exp	experimental
ext	external
f	final
fib	Fédération Internationale du Béton
gen	generalized
i.e.	*id est*
int	internal
ult	ultimate
vp	viscoplastic

Symbols

The following list of symbols is organized by chapter and presented in appearance order:

Chapter 2: State of the Art

l_b	minimum tie length
Ω_{steel}	steel cross sectional area
f_{yd}	design yield limit stress
F_{Sd}	design reaction force

Chapter 3: Computational Developments

x	corotated horizontal axis / local reference system
z	corotated vertical axis / local reference system
X	global horizontal axis
Z	global vertical axis
$\mathbf{q}_{global}^{T}$	vector of displacement components in the global reference system
u_1	horizontal displacement of node 1 in the global reference system
u_2	horizontal displacement of node 2 in the global reference system
w_1	vertical displacement of node 1 in the global reference system
w_2	vertical displacement of node 2 in the global reference system
θ_1	rotation of node 1 in the global reference system
θ_2	rotation of node 2 in the global reference system
$\mathbf{q}_{local}{}^{T}$	vector of displacement components in the local reference system
$\bar{u}$	axial displacement in the local reference system
$\bar{\theta}_1$	rotation of node 1 in the local reference system
$\bar{\theta}_2$	rotation of node 2 in the local reference system
$\bar{u}$	axial displacement in the local reference system
$\bar{\theta}_1$	rotation of node 1 in the local reference system
$\bar{\theta}_2$	rotation of node 2 in the local reference system

α	angle of rigid body rotation
β	current angle between the element and the global reference system
β_0	original angle between the element and the global reference system
X_1	horizontal coordinate of node 1 in the global reference system
X_2	horizontal coordinate of node 2 in the global reference system
Z_1	vertical coordinate of node 1 in the global reference system
Z_2	vertical coordinate of node 2 in the global reference system
c_o	cosinus of the original angle between the element and the global reference system
s_o	sinus of the original angle between the element and the global reference system
c	cosinus of the current angle between the element and the global reference system
s	sinus of the current angle between the element and the global reference system
L	element undeformed lenght
l_f	element deformed lenght
l	element undeformed lenght at the begining of each increment
$\mathbf{f}_{local,\mathrm{int}}$	local internal force vector
$\bar{N}$	normal internal force
$\bar{M}_1$	internal moment applied to node 1
$\bar{M}_2$	internal moment applied to node 2
f_1^X	horizontal internal force in the global reference system applied at node 1
f_1^Z	vertical internal force in the global reference system applied at node 1
c_1	internal moment in the global reference system applied at node 1
f_2^X	horizontal internal force in the global reference system applied at node 2
f_2^Z	vertical internal force in the global reference system applied at node 2
c_2	internal moment in the global reference system applied at node 2
$\mathbf{T}$	transformation matrix
$\mathbf{K}$	tangent stiffness matrix
$\mathbf{f}_{global,\mathrm{int}}$	global internal force vector
$\mathbf{f}_{local,\mathrm{int}}$	local internal force vector
$\mathbf{t}_1$	first line of the transformation matrix $\mathbf{T}$
$\mathbf{t}_2$	second line of the transformation matrix $\mathbf{T}$
$\mathbf{t}_3$	third line of the transformation matrix $\mathbf{T}$

$\mathbf{r}$	auxiliary vector $\mathbf{r}$
$\mathbf{z}$	auxiliary vector $\mathbf{z}$
$\mathbf{q}_{global}$	vector of displacement components in the global reference system
$\mathbf{K}_{local}$	local tangent stiffness matrix
u_{local}	local axial displacement
w_{local}	local vertical displacement
$\bar{\varepsilon}$	axial strain
χ	curvature
$\mathbf{E}^{gen}$	vector of generalized strains
ε	total axial strain
a_{cor}	element cross sectional area in the corotated axis
σ	one-dimensional normal stress
N	normal force
M	bending moment
v_{cor}	element volume in the corotated axis
W_{int}	internal work
i	number of the layer
ε_i	total axial strain at a fixed position x, for a given layer i
u	local axial displacement, with the suppression on the index $local$
$\bar{z}_i$	position of the gravity center, for the cross section a given layer i
$\sigma_{i,conc}$	one-dimensional normal stress on concrete, for a given layer i
$\sigma_{i,steel}$	one-dimensional normal stress on steel, for a given layer i
$\sigma_{i,total}$	total normal stress, for a given layer i
Ω_i	total cross sectional area, for a given layer i
$\Omega_{i,steel}$	cross sectional area of steel, for a given layer i
$\mathbf{B}$	matrix of the derivatives of the local shape functions
H_i	consistent tangent operator, for a given layer i
$\mathbf{H}$	sectional consistent tangent operator
$\mathbf{\Sigma}^{gen}$	vector of stress resultants
$\sigma_{h,conc}$	current maximum compressive stress
$\sigma_{0,conc}$	initial maximum compressive stress
μ	softening parameter, for concrete
κ_{conc}	cumulated plastic strain, for concrete
$\sigma_{h,steel}$	current yield limit
$\sigma_{0,steel}$	initial yield stress
η	hardening parameter, for steel
κ_{steel}	cumulated plastic strain, for steel
$\mathbf{K}_T$	structural tangent operator
$\mathbf{f}_{int}$	internal force vector

q	vector of nodal displacements
q̇	vector of nodal displacement rates
M	mass matrix
q̈	vector of nodal accelerations
$\mathbf{f}_{ext}$	vector of external forces
$\dot{\varepsilon}^{vp}$	viscoplastic strain rate
λ	viscosity parameter
f	overstress function
$\sigma_{0,mat}$	material (steel or concrete) initial yield/maximum compressive stress
n	viscosity parameter
$\sigma_{mat}]$	one-dimensional stress, for concrete or steel
$\bar{\sigma}_{mat}$	current yield stress / maximum compressive stress
$\langle ... \rangle$	MacAulay brackets

Chapter 4: Quasi-Static Analysis of Monotonically Loaded Planar Frames

ϕ	diameter
h	height
f_c^{exp}	experimental average compressive strength
$\sigma_{0,steel}$	steel yield strength
$\sigma_{ult,steel}$	steel ultimate strength
$\varepsilon_{ult,steel}$	steel ultimate strain
η	hardening parameter, for steel
E_{steel}	steel Young' modulus
$\varepsilon_{ult,conc}$	concrete ultimate strain
f_c'	maximum concrete compressive strength
E_{conc}	concrete Young's modulus
κ_{conc}	cumulated plastic strain, for concrete
μ	softening parameter, for concrete
F	point load simulating gravity loads
N	point load simulating the presence of a column
P	structural section
Q	structural section
$P_1, P_2, ...$	points on the *Load versus Displacement* curve

Chapter 5: Design Code Comparison and Dynamic Progressive Collapse Analysis of a Five-Store Building

q_{dead}	self-weight load, for reinforced concrete beams
A, B, C, D, E	structural sections
V_1	vertical displacement of the Eurocode-based frame
V_2	vertical displacement of the NBR-based frame
$P_1, P_2, ...$	points on the *Vertical Displacement versus Time* curve
ω	structure's natural frequency
k	structure's stiffness
m	structure's mass
.	section of steel yielding
$\bigtriangledown$	section of concrete crushing (more than 30 %)

Chapter 1

Introduction

Progressive Collapse (PC) is a catastrophic structural behavior of buildings that leads to financial losses and regretfully, sometimes to human losses. It happens when a structural key element is irreversibly damaged, forcing the remaining structure to redistribute loads which, in turn, leads to the damage of other structural elements. This cycle of damage-load redistribution can result in the stabilization of the remaining strucuture or in the total collapse of the building (MARJANISHVILI [1]).

Provided exceptions, the PC triggering event is usually characterized by its reduced magnitude when compared to the actual final result. Although the cause of the initial failure varies from case to case, the following classification applies (MASOERO *et al.* [2]):

- **accidental event** - resulting from a coincidence of factors that induces the failure of one or more key structural elements. These factors can be associated to natural or human-induced occurrences as, for instance, flooding, extreme snow/wind load, earthquakes, gas explosion, car crash, etc.. In some cases, accidental events can be foretold and have their effects mitigated, if not completely eliminated;

- **intentional event** - previously planned action whose main purpose is to cause the ruin of a building or part of it. In this case, the PC is not only the result but the objective of causing the failure of predetermined structural elements. Demolition processes and terrorist attacks are the most evident examples of intentionally produced PC.

1.1 Cases of Progressive Collapse

The literature provides several examples of progressive collapse around the world. Three classic examples are described below, along with some cases in Brazil:

• **Ronan Point (London, 1968)**

Typically residential, Ronan Point apartment building was 64 meters high and its 110 apartments were distributed in 22 floors which had just been opened for occupation (Fig.1.1). Stairs and floors consisted on prefabricated concrete panels, usual to the Larsen - Nilsen system (PEARSON and DELATTE [3]), and walls were designed to behave as structural elements.

Fig. 1.1. Ronan Point collapse [4]

The initial failure was accidentally caused by a gas explosion in the kitchen of apartment 99, located on one of the corners of the building (PEARSON and DELATTE [3]). Without adequate load-bearing support, the kitchen's floor and walls ruined. Thus, the PC characteristic domino effect started and lead to the collapse of the upper floors (VLASSIS [5]).

The successive redistribution and increasing of loads on the lower floors, due to self-weight and impact of the debris, gave continuity to the failure (VLASSIS [5]). As shown in Fig. 1.1, the modular nature of the constructive system kept the effects of the explosion to one sector of the building, which was later rebuilt. Four people died as consequence of Ronan Point collapse. Financial losses included the immediate devaluation of other nearby buildings that used the same constructive

system and the premature demolition of the affected building and eight identical others (MITAL *et al.* [6]).

An investigation group was created to evaluate the structural causes of the failure and concluded that connections between walls and floors were not sufficiently strong to overcome the explosion load. This insufficiency resulted, among others, from non-observance of design specifications, inadequate quantity of mortar applied to the joints and excessive torque on screws and bolts (VLASSIS [5]). The explosion itself was considered to be within the expected magnitude of a domestic incident. However, the equivalent wind load resulted in a 2% failure probability within 60 years, shorter than the expected lifetime of the structure. Building codes did not included the assessment of PC potential at that time and modifications of the British building codes were proposed after this event (PEARSON and DELATTE [3]).

- **Murrah Office Building (USA, 1995)**

The 18-year old governmental building was built in reinforced concrete (RC) and had a projected area of 2045 square meters (Fig. 1.2). Its 40 meters height was not equally distributed along the nine floors: the first two had total height of 12.2 meters; the ninth floor, 4.3 meters; the others, 4 meters each. A special transfer girder made possible the significant height difference observed for the first floors, reducing the load on the columns (VLASSIS [5]).

Fig. 1.2. Murrah Office - before [7]

The initial failure was intentionally caused by the explosion of a truck carrying a load of fertilizer, equivalent to 1800 kg of dynamite. The sequential failure that succeeded the explosion fits the PC definition. Three columns were considerably damaged, leading to the destabilization of other structural elements and starting the characteristic PC cycle. The reduced support capacity of these columns and the resultant incapacity of load redistribution led to the ruin of the upper floors. Due to the accumulated load, the transfer girder and adjacent elements collapsed (VLASSIS [5]).

Besides the damage to approximately 25% of the Murrah Office Building (Fig. 1.3), around 300 other buildings were affected and 168 people were killed (NPS [8]). According to HOFFMAN [9], up to 680 million dollars were spent on restructuring the area, including the demolition of the remaining Murrah Office Building, investigation work on the attack and the construction of a nation memorial and museum.

Fig. 1.3. Murrah Office - after [10]

After the event, the American Department of Justice decided to elaborate codes for reinforcing and protecting existing buildings against similar attacks. The General Service Administration (GSA) was in charge of coordinating these studies and proposed a five category classification for government buildings according to the size, the number of employees and the volume of external access associated to each building, among others. The resultant report was denominated GSA Security Design Criteria (GSA [11]) and has been accepted as an evaluation guideline for the safety

of public building in USA ever since. This guideline included not only design and building recommendations, but also recommendations on safety systems, operations and equipments that would allow preventing terrorist attacks, evacuating the place and assisting the victims (NADEL [12]).

- **World Trade Center (USA, 2001)**

The financial complex known as World Trade Center (WTC) was composed by seven buildings including the world famous Twin Towers (Fig.1.4), considered the tallest buildings in the world until 1974 (more than 410 meters each). The weight of each tower was as high as 500 thousand tons while the wind load was equivalent to 5 thousand tons. Their core consisted on a highly hyperstatic system of 244 steel columns, defining an empty space for hoistways and stairs. The construction of these buildings in the Manhattan island occurred between 1960 and 1970, constituting an investment of approximately 350 billion dollars. Private companies and governmental agencies had offices in the WTC, where restaurants, hotels and TV towers were also installed (FEMA [13]).

Fig. 1.4. Construction of the World Trade Center [14]

The initial failure was caused by a terrorist attack in which hijacked airplanes, two boeings 767-200ER, were flown into the towers, leading to their ruin. Many factors composed the critical failure scenario that resulted in the collapse of the towers as, for example, the impact of the airplanes, the fire caused by fuel explosion, the increasing and consequent reallocation of loads, etc. The first airplane hit the North Tower between the 94th and the 98th floors and, 103 minutes latter, the tower

collapsed (Fig. 1.5). Meanwhile, another airplane hit the South Tower between the 78th and the 84th floors (Fig. 1.6). The Second Tower also withstood the impact but collapsed after 56 minutes. The other five buildings belonging to the WTC complex were affected by the collapse of the Twin Towers. Besides, other 49 neighbouring buildings were damaged (FEMA [13]).

Fig. 1.5. Collapse of the North Tower [15]

Fig. 1.6. Collapse of the South Tower [16]

The economical losses associated to the attack to the WTC were estimated to be as high as 70 billion dollars, which classifies the event as one of the largest economical catastrophes in USA (COPPOLA *et al.* [17]). Official numbers account for more than 3000 victims. The successful evacuation of the lower levels was only possible because the towers remained stable for a long time after the attacks, allowing the removal of 95% of the occupants (FEMA [13]).

Over the years after the attack, many modifications were proposed for engineering, safety and security matters based on the analyses of the event. For instance, a report from the National Institute of Standards and Technology (NIST [18]) describes the design, the project, the construction and the maintenance of the WTC complex, as well as the building codes applied to its construction in the 60's. It also depicts the attacks and the evacuation procedures, and presents thirty recommendations for improving structural safety, fire safety and well being of the users. In 2008 and 2010, based on NIST's report (NIST [18]), the International Code Council (ICC) approved 41 changes in international building and fire safety codes (FACILITIESNET [19]). Although none of these changes addresses the PC of buildings, one of them can be associated to structural improvement, recommending the use of floor slabs with no direct connection with the columns.

● **Progressive Collapse in Brazil**

Also in Brazil there were occurrences that can be associated to PC. The failure of the Real Class (Belem/2011, Fig. 1.7) and the Liberdade (Rio de Janeiro/2012, Fig. 1.8) made the news all over the country. Months after the buildings collapsed, newspapers pointed out that inappropriate design and poor execution were responsible for the failure of the former (LIMA [20]), while careless structural modifications were believed to have caused the ruin of the latter (COURI and DEUTSCH [21]). However, the official reports are not available to the main public, since the cases are still *sub judice*.

Fig. 1.7. Real Class: before and after [22]

Fig. 1.8. Liberdade: before and after [23]

Other examples of PC related occurrences in Brazil are presented below:

- **Luiz de Queiroz Building - COMURBA**

The partial collapse of the building occurred in Piracicaba/São Paulo, in 1964, killing 54 people. It is considered the first engineering disaster in Brazil and, still today, the causes remain unknown (GARCIA [24]). Figures 1.9 and 1.10 present the before-after scenario of the once known as COMURBA (Companhia de Melhoramentos Urbanos).

Fig. 1.9. COMURBA before [25]

Fig. 1.10. COMURBA after [26]

- **Palace II Building**

The building was located in the city of Rio de Janeiro and collapsed in 1998 (Fig. 1.11). The event, caused by mistakes in both design and construction processes, killed 68 people. The main cause of the collapse was the failure of undersized columns (31 out of 41 columns were smaller than what an appropriate design would require). Minor problems were also identified: insufficient concrete layer covering the steel reinforcement bars; lack of steel hooks for anchoring the reinforcement bars; steel corrosion and high levels of porosity in the concrete (OLIVEIRA [27]).

Fig. 1.11. Palace II collapse [28]

● **Building collapses in Pernambuco**

In the last 30 years, more than 15 collapses were registered in the metropolitan region of Recife, capital of Pernambuco (Fig. 1.12). The Instituto de Tecnologia de Pernambuco states that 5300 building in that region apply a self-suport assemblage method known as *caixão* (GLOBO [29]). These structures are not always designed/built by specialized professionals and, most frequently, lay people are responsible for the complete procedure, from defining the architecture and structural elements to the construction process itself (MELO [30]).

Fig. 1.12. Collapse in Recife [31]

Some of these Brazilian cases are examples of bad, non-professional processes of design and/or execution. These uncontrolled PC scenarios are composed by unpre-

dictable variables and are, therefore, difficult to reproduce. This work, as presented in the following, focuses on buildings that were correctly designed and executed and on their behavior to the removal of a column.

1.2   Main Contributions and Originality

This work establishes a direct correlation between a numerical effort and quasi-static experimental studies of PC, which is quite rare in the best knowledge of the author. The numerical assessment of PC response of two RC structures is proposed. These experiments were performed by other authors and the experimental data is available in the literature (LEW *et al.* [32], YI *et al.* [33]). Within the significant body of literature concerning experimental tests, the selection of these structures was made considering: (*i*) the amount of available information on the experimental conditions (geometry, constituent material parameters, loading pattern, PC simulation details) that would allow the direct numerical representation of the laboratory tests; (*ii*) the available information on the experimental structural response, in which different failure mechanisms and the sequence of their appearance had been clearly identified.

The proposed beam element incorporates geometric nonlinearities in large displacements through the use of a corotational reference system (CRISFIELD [34], BATTINI [35]). A multilayer discretization on the sectional level (IRIBARREN *et al.* [36]) is used for linking strains and stresses and allows accompanying the gradual concrete crushing in the beam depth, as well as the reinforcement bar yielding and final failure. Nonlinear one-dimensional constitutive laws are used to represent concrete and steel behavior (CEN [37], *fib* [38, 39]). To the best knowledge of the authors, the study of PC scenarios under the combination of a corotational beam formulation and a multilayer cross sectional discretization with the ingredients presented herein was not used before, and its application along with experimental comparisons represent an originality in this work.

The majority of works concerning the verification of progressive collapse usually considers structural designs based on European, North American or Asian Building codes. A deep literature review shows that the type of progressive collapse verification proposed here was not attempted before for buildings that follow the structural recommendations of the Brazilian codes. The application of the resulting computational tool to the comparison between two structures following different building codes, European and Brazilian, but having identical architectural geometry is also an originality of the presented work.

1.3   Scope of the Thesis

The study of the PC of reinforced concrete buildings is the main subject of this thesis, which is organized as follows: the second chapter is a bibliographical review, aimed at discussing PC code provisions and experimental/computational works. The review focuses on features that directly relate to the formulations described hereafter. The third chapter describes the implementation of an element, based on the Bernoulli beam theory. The formulation is derived within a corotational description of the kinematics of the element which is coupled to a multilayer discretization of the transverse sectional area. The modeling of the material constitutive behavior is also presented, as well as the procedures for the solution of the nonlinear dynamic problem. The fourth chapter consists of a direct correlation of experimental results selected from the specialized literature and the ones obtained with the application of the Bernoulli beam element. These results aim at approaching PC via the analysis of reinforced concrete frameworks that represent portions of realistically designed buildings. The Bernoulli beam element is also used in the fifth chapter to establish a comparison of the PC behavior of a building designed in accordance to two different building codes, EUROCODE [37] and NBR 6118 [40]. Finally, concluding remarks and perspectives for future works are presented on Chapter 6.

Chapter 2

State of the Art

This chapter presents a bibliographic review concerning experimental and numerical Progressive Collapse (PC) simulations. It also includes a summary of the building codes provisions related to the PC of reinforced concrete (RC) buildings. The criteria adopted to construct this chapter was identifying works that somehow share a connection to the formulation and/or simulation proposed herein.

2.1 Experimental Approaches

Experimental efforts are specially interesting because they allow the investigation of the true behavior of the materials in the structures. Another advantage comes from the fact that this approach makes it possible to observe the sequencing of events that leads to the final collapse. Experimental tests also have the advantage of reflecting the coupling of many different effects in one source, which means that the test models behavior is very similar to the behavior of the structures built in everyday practice. Besides, experimental PC analysis permits the examination of outcomes whose occurrence is naturally random as, for instance, the disposition of the debris.

However, these same advantages may constitute the main disadvantages of the experimental analysis. First, the behavior of one model is very unique and strictly refers to that specific model. The general conclusions are usually inferred from that behavior and extrapolated to other models. This reflects another limitation: practical complications implied in building and destroying experimental specimens make this type of investigation impossible to perform systematically for a large range of structures. This disadvantage justifies the efforts employed on modelling of PC computationally (GOUVERNEUR *et al.* [41]). In addition, since all effects are coupled, it is difficult to isolate one for investigating its influence in the final results. Finally, the experimental approach is expensive due to the necessary amount of time, space, human and, of course, financial resources that are required.

In recent years, a large number of experimental studies were carried out to investigate how RC frame structures behave when subjected to column failure. On one hand, some of these works are focused on studying the dynamic response of the whole building when one or more vertical supports are suddenly removed by blast loading (SASANI *et al.* [42, 43]). However, the initiation of collapse can also be performed by slow column demolition, taking into account only the static behavior of the structure (KOKOT *et al.* [44]). Other experimental studies are focused on investigating only the behavior of a part of a structure, usually a beam-column assemblage subjected to column loss (LEW *et al.* [32], YI *et al.* [33], QIAN and LI [45], SADEK *et al.* [46], SU *et al.* [47], SASANI and KROPELNICKI [48]). In this case, the removal of the vertical support is usually performed in a quasi-static manner by applying a monotonically increasing displacement (monotonically decreasing reaction force) at the connection with the failed member.

LASKAR *et al.* [49] used piezoceramic-based devices (smart aggregates) to monitor and locate the formation of plastic hinges (PH) in a two-story RC frame. The author stresses that, in a PH based analysis, the information on the quantity, location and maximum deformation capacity of these PH constitutes information on the structural failure itself and, consequently, on the PC of the structure. Results assured the effectiveness of the smart aggregates as monitoring tools.

The experimental investigations of YU and TAN [50] on RC sub-assemblages aimed at comparing structures that were designed with and without seismic detailing. The adopted instrumentation allowed observations at three different geometric levels: structural level, sectional level and fiber level (points on the cross section). The authors demonstrate that structural resistance increases with the development of compressive arch action and catenary effects.

GOUVERNEUR *et al.* [41] point out that experimental tests focusing on membrane actions in slabs are much more common then the ones concerning catenary actions and propose a setup for testing RC hyperstatic strips. The results confirm that catenary effects increase the structural robustness, enhance the load-bearing structural capacity and, therefore, help mitigating the occurrence of progressive collapse in RC structures.

Progressive collapse and membrane actions in RC concrete beams are also experimentally investigated by FARHANGVESALI *et al.* [51]. The authors study the influence of varying the transversal/longitudinal reinforcement ratio, the maximum compressive strength of concrete and the effects of strain penetration. Strain penetration of longitudinal reinforcement bars, also known as bond-slip, "causes a pinching effect in the column's hysteresis", reducing its stiffness and increasing the deformation in dynamic scenarios (KO and PHUNG [52]). The results of FARHANGVESALI *et al.* [51] show that the peak load capacity of RC beams is not strongly affected by

variations of either the longitudinal reinforcement ratio or the configuration of the transversal reinforcement, provided minimum requirements are met. Signs of strain penetration were identified in the experiment and were shown to affect the stiffness of the beams. In view of the results, the authors point out that strain penetration should be taken into account when estimating initial stiffness and loading capacity of RC beams.

2.2 Numerical Modelling

The number of works related to the numerical investigation of the progressive collapse of RC structures is large and include an extensive variation of objectives within the theme. Marjanishivilli [1] divides PC numerical analysis methods in four groups: linear static, nonlinear static, linear dynamic and nonlinear dynamic. In an experimental program, dynamic and nonlinear effects are always convoluted and the various effects which are involved in the PC (plasticity, vibrations, concrete crushing, steel breaking, etc.) are coupled, making it difficult to individually study the behavior of structures following the classification proposed by Marjanishivilli [1]. On the other hand, numerical approaches present the advantage of allowing several simulations in a relatively short period of time and at significantly reduced cost with respect to the experimental approaches. This advantage also allows parametric studies to be performed for a deeper understanding of the structural behavior of the models and for studying the influence of isolated material parameters without requiring a new test specimen for each of the variations of the studied parameter.

Considering that RC is a composite material exhibiting important microstructural effects related to the reinforcement, the response of RC frames is strongly dependent on the reinforcement scheme and steel quantity. Besides, isolating the effects of concrete crushing, steel yielding and/or steel fracture is important although their separate influence is usually difficult to capture. Multiscale approaches are a natural way of incorporating features of the material microstructure in the numerical assessment of the progressive collapse of RC structures. The layer discretization of a section, *i.e.*, dividing the transversal section of the element into layers, for numerical computation, is an example of multilevel analysis. These approaches have been used in different contexts of RC analysis, as for example, by SPACONE *et al.* [53, 54], who presents a fiber beam-column element for nonlinear dynamic analysis considering cyclic combinations of bending moments and axial forces. The authors propose a general algorithm for, given the end deformations of an element, obtaining the stiffness matrix and the resisting forces. Another nonlinear fiber beam element, this time accounting for cyclic bending and shear, is proposed by PETRANGELI *et al.* [55] and PETRANGELI [56]. The importance of having an efficient integration

of sectional forces and deformations along the length of the element is stated and, based on that statement, a strain field method is presented. Strain field methods are used to describe the deformation of a given solid and, according to BIAN *et al.* [57], assume:

- solid objects with no voids;

- material homogeneity and isotropy;

- stresses in the undeformed state are equal to zero;

- deformations are small and proportional to the applied forces;

- if forces are removed, the body returns to the undeformed configuration.

A multifiber element for three-dimensional analysis of RC structures is brought by MAZARS *et al.* [58]. The element is based on the Timoshenko beam theory and includes the uncoupled effects of shear and torsion. The introduction of warping in the nonlinear analysis of beams under torsion is shown to positively alter the results in terms of torque-rotation evolution. Long-term deformations of RC structures is addressed by BACINSKAS *et al.* [59], who proposed a layer-based technique for the evaluation of concrete crushing, creep, tension-stiffening and shrinkage in a time-dependent analysis. A combination of the Timoshenko beam theory, the multilayer discretization and the Modified Compression Field Theory (MCFT) was proposed by STRAMANDINOLI and LA ROVERE [60] in order to consider shear effects and the transversal reinforcement. The MCFT was based on experimental testing of RC panels loaded and used for predicting the behavior of these panels under pure shear or shear/axial stress (BENTZ *et al.* [61]). STRAMANDINOLI and LA RO-VERE [60] call the attention to the fact that the Timoshenko beam model usually demands more computational effort, which is a result of a higher number of iterations at each loading step. Despite their particularities, these multifiber/multilayer works also have in common the practice of validating their results by using, at least, one experimental-numerical comparison. Therefore, the literature shows that multifiber approaches apply physically-based models, allowing for direct comparison with experimental data.

There are cases in the literature in which the the plastic hinge method (PHM) is applied to the PC analysis of reinforced concrete buildings (KOKOT *et al.* [44, 62]). However, according to IRIBARREN [63], layer/fiber discretization may be preferable if one considers the main limitations of the PHM, among others:

- the need to define *a priori* cross sectional properties and generalized constitutive laws as well as the position of the hinges, making it unpractical to perform

parametric studies, *i.e.*, different bending moment *versus* curvature relationships $(M(\chi))$ have to be postulated for all different cross sections in the structure;

- constrained plastic strain evolution, since the position of the hinges and their behavior are usually, but not always, set *a priori*;

- the difficulties for representing complex coupled effects, as the $M(\chi)$ relationships usually postulated remain largely independent of the axial force, for instance.

Some of the already discussed experimental works show that geometric nonlinearities have an important role in the analysis of PC (GOUVERNEUR *et al.* [41], YU and TAN [50], FARHANGVESALI *et al.* [51]). Other numerical investigations also focus on the impact of nonlinear geometric effects on the collapse of structures. BAO *et al.* [64] presented a simplified macromodel-based approach to investigate RC large displacement framework. Discrete nonlinear springs were used for simulating the connections between beams and columns. The work affirms the viability of macromodeling approaches in opposite to detailed finite-element analysis. However, the authors state that this success is dependent on the careful calibration of the spring properties and, consequently, the macromodel itself. According to the authors, this calibration is still a challenge since no sufficient experimental data is available. DAT and HAI [65] numerically investigated the membrane effect on a beam-slab structure after the loss of a penultimate-internal column. Sixteen cases, which differ in terms of restraining boundary conditions and reinforcement schemes, were analysed. Results show that the membrane effect (and also the catenary effect) has significant influence on enhancing the load-bearing capacity of beam-slabs substructures, in some cases, doubling the flexural capacity.

ELKOLY and EL-ARISS [66] proposed a cable scheme for mitigating the occurrence of progressive collapse in RC buildings. The system of plastic cables is positioned laterally to the beams and aims to strengthen the structure by taking advantage of the catenary effects. The authors justify the choice for plastic cable based on their lighter weight when compared to steel cables/rods and also on their high resistance to corrosion and other chemical attacks. Besides, the cables are not post tensioned, allowing their use on the reinforcement of pre-existing structures. Parametric studies were performed considering different types of cables, cable geometries and cable systems. The numerical analyses show that the proposed cable systems are successful in improving structural behavior associated to column loss.

KEYVANI *et al.* [67] demonstrated the increase of the punching strength as an effect of the compressive membrane actions in RC slabs. Experimental data from the literature were used to validate the numerical developments. The work shows that analysis based on fully restrained slabs tends to overestimate the enhancement of punching strength and that the anchorage of tensile bars in experimental works

might not correspond to the ones practiced for real-life structures, also leading over-estimation of the punching strength.

XU and LIU [68], who specifically investigate the PC of RC frames caused by explosions, calls the attention to the complexity of the structural response involving blast loads and the consequent shock waves interactions. According to the authors, two stages can be identified: the failure of key elements and the following structural response to that failure. It is concluded that the instantaneous removal of the failure members affected by explosion is feasible in numerical simulations. Besides, the work reveals the importance of strengthening structural connections as a PC mitigation practice. No information is given on the numerical method used for modelling the problem.

MASOERO *et al.* [2] investigate the behavior of RC frames after the removal of a column in terms of final collapse extent and fragment size distribution. Parametric studies relating cross sectional size, reinforcement ratio/arrangement and plastic capacity of the structural members are presented. Asymmetric arrangement of the reinforcement is shown to contribute to partial localized structural failure. The work shows that, when considering slender structural elements, the lower the plastic capacity, the larger is the damage propagation due to fragment depositing and cutting of ground columns. The same is not necessarily true for more robust columns. On the other hand, lower plastic capacity also contributes to smaller sized fragments which might be an advantage in the case of controlled demolition.

2.3 Building Codes Provisions on Progressive Collapse

Different building codes are used worldwide to define the rules for building in reinforced concrete. Some of these building codes provide information on how to mitigate the risks related to progressive collapse, as exemplified in the following. Nevertheless, none of these codes imposes nor indicates any method for numerical analyses.

The American Concrete Institute (ACI [69]) does not namely address the problem of the PC of reinforced concrete buildings. However, section '7.13 Requirements for Structural Integrity' is aimed at presenting ways of improving integrity by improving structural redundancy and ductility. ACI [69] recommends, for instance, the continuity of at least two beam tension reinforcements, which contributes to the development of catenary actions and to a better distribution of the load after localized failure. In order to guarantee adequate continuity of the reinforcement, the code also prescribes appropriate positioning of splices, when those are necessary.

Section '1.4 General Structural Integrity' on American Society of Civil Engineers' ASCE [70] provides guidelines to obtain minimum interconnectivity between structural elements and to create a lateral force-resisting system to make buildings able to withstand the design loads and to remain stable after unforeseen events such as fires, explosions and vehicular impact. Since Section '2.5 Load Combination for Extraordinary Events' specifies that the code applicability does not include disproportionate collapse, it is understood that the code directly applies to localized failure only. The understanding is correct when compared to the the 'Commentary' section of the same document (non-mandatory), in which it one reads: '*ASCE does not intend, at this time, for this standard to establish specific events to be considered during design or for this standard to provide specific design criteria to minimize the risk of progressive collapse*'.

The 'Commentary' section on ASCE [70] also makes a distinction between the direct and the indirect approaches for mitigating the occurrence of PC. The direct approach assumes that the structure is explicitly designed to overcome the loss of a structural member (Alternate Path Method-APM) or the effects of an abnormal load applied to an specific point of the building (Specific Local Resistance Method - SLRM). As for the indirect approach, however, a set of qualitative procedures is defined to obtain minimum levels of strength, continuity and ductility. These procedures include, for instance, defining a good plan layout, compartmentalizing the structure, designing redundant structural systems and accounting for the catenary actions of the floor slabs.

Buildings are classified by the Department of Defense of the United States (DoD) into four categories (DoD [71]), according to the occupancy level proposed by DoD [72]. The Occupancy Level was introduced in 2013 as a substitute to the former Protection Level, becoming the reference for identifying the required level of PC design. From the lowest to the highest occupancy levels (I to IV), different design requirements are proposed, including the application of the APM and the SLRM or, as defined by DoD [72], Enhanced Local Resistance Method (ELRM). For some structures, the document also prescribes the application of the Tie Force Method (TFM), which requires the building to be mechanically tied together in order to create alternative load paths and produce the adequate continuity and ductility via the floor/roof systems. The document stipulates specific requirements and load combination schemes for each of the three methods and also considers their application to different materials as, for example, wood, reinforced concrete and steel. Other important modifications were added to DoD [71] in 2013: an Appendix with key terms and concepts of structural analysis, inclusion of increase factors for static models and the replacement of the Additional Ductility Requirements for the already mentioned ELRM.

The 2013 version of '*GSA Progressive Collapse Analysis and Design Guidelines for New Federal Office Buildings and Major Modernization Projects*' (GSA [73]) is, as it describes itself, an attempt to 'bring alignment within the industry by reducing incongruities between GSA and DoD methodologies' (GSA [74]). A description of which structural elements are to be removed in a PC analysis, including cases where multiple removal must be considered and minimum redundancy requirements for withstanding the element removal are included in GSA [74].

In this new version of GSA [73], the guidelines no longer include the Tie Force Method or the Enhanced Local Resistance Method and are almost entirely based on the Alternate Path Method proposed by DoD [71] for different materials. Another significant difference in relation to the 2003 version is that GSA [74] is now threat dependent and should be used in parallel with the American Interagency Security Committee's ISC [75] and the blast criteria GSA [76]. The latter prescribes detailed information on implementing explosions and on PC requirements but it is not available to the general public.

Section '10.3 Estados Limites Últimos (ELU)' on NBR 6118 [40] specifically establishes that the safety of reinforced concrete structures must always be verified against: the limit states related to the depletion of the resistant capacity in the complete structure (and in its individual structural elements) considering, among others, the geometrically nonlinear effects; the limit states caused by dynamic loads and; the progressive collapse limit state. NBR 6118 [40] also defines the appropriate flexural reinforcement and the minimum tie length (l_b) for guaranteeing local structural ductility against progressive collapse (FIG. 2.1).

According to NBR 6118 [40], the adequate reinforcement area (Ω_{steel}) must comply with:

$$\Omega_{steel}\, f_{yd} = F_{Sd} \tag{2.1}$$

where f_{yd} is design yield limit stress and F_{Sd} is the design reaction force. As shown in FIG. 2.1, the minimum tie length is supposed to be added to the quantity C or C' values, which depend on the cross section of the column. These specifications are made only for flexural reinforcement of RC slabs and other structural components with $w_{cross} \geq 5d_{cross}$, where w_{cross} and d_{cross} are the cross sectional width and useful height, respectively. These characteristics usually do not apply to either RC beams or columns.

Section '5.1 Processos de cálculo' on NBR 9062 [77] states that special measures concerning the general structural organization and the constructive details must be taken in order to prevent the PC of precast concrete structures. Nonetheless, these special measures are neither defined nor specified. The complementary documents
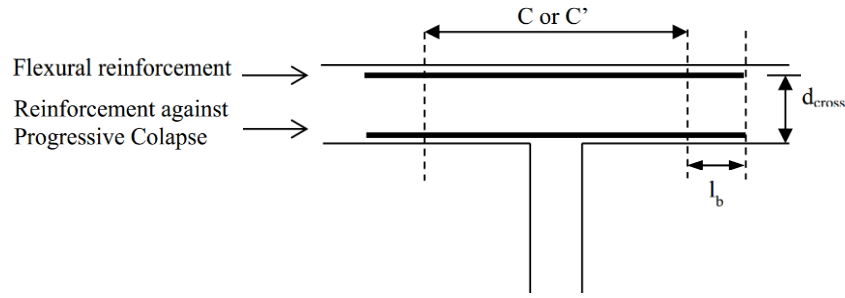
Fig. 2.1. Reinforcement against Progressive Collapse

indicated by NBR 6118 [40] and NBR 9062 [77] are vague on the PC subject or make no reference to the problem.

EUROCODE [78] defines load values and load combinations to be considered in the design and analysis of civil engineering works. It is divided into four parts that cover loads of different nature (self-weight, fire, wind, snow, traffic loads, *etc.*). EUROCODE [78] also "provides strategies and rules for safeguarding civil engineering works against ... accidental actions", including the progressive collapse of buildings due to the impact of cars and internal explosions, among others. These strategies are based on identified accidental actions and on limiting the extent of localised failure (FIG. 2.2), which is shown in FIG. 2.3.
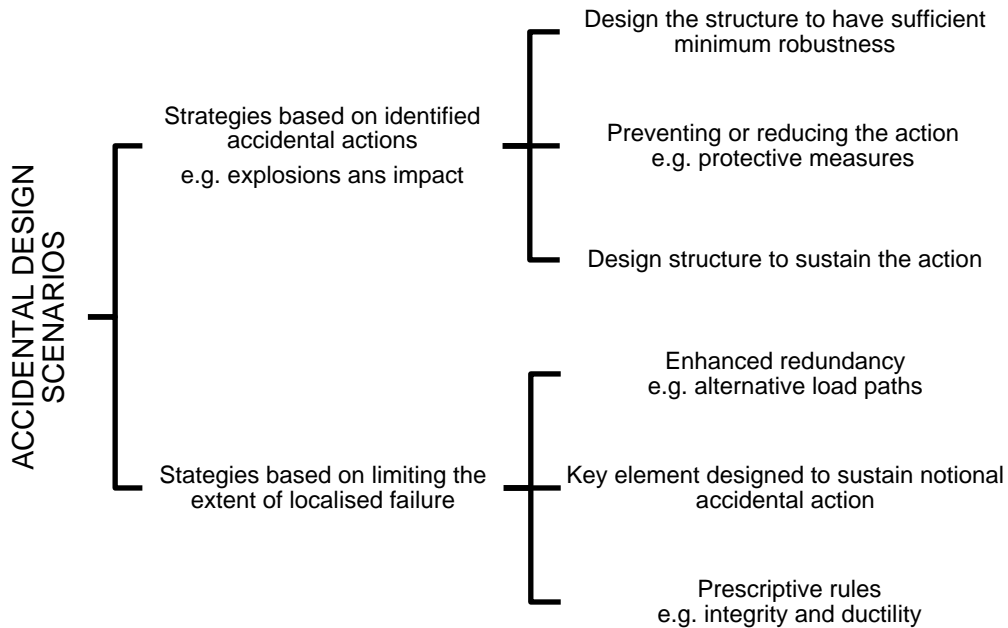
Fig. 2.2. Accidental design scenarios and strategies

Depending on the consequences of their failure, buildings are classified by EUROCODE [78] as CC1, CC2 or CC3, which stand for low, medium and high consequence class, respectively. As seen on Table 2.1, different approaches are recommended for each one of these classes.

20
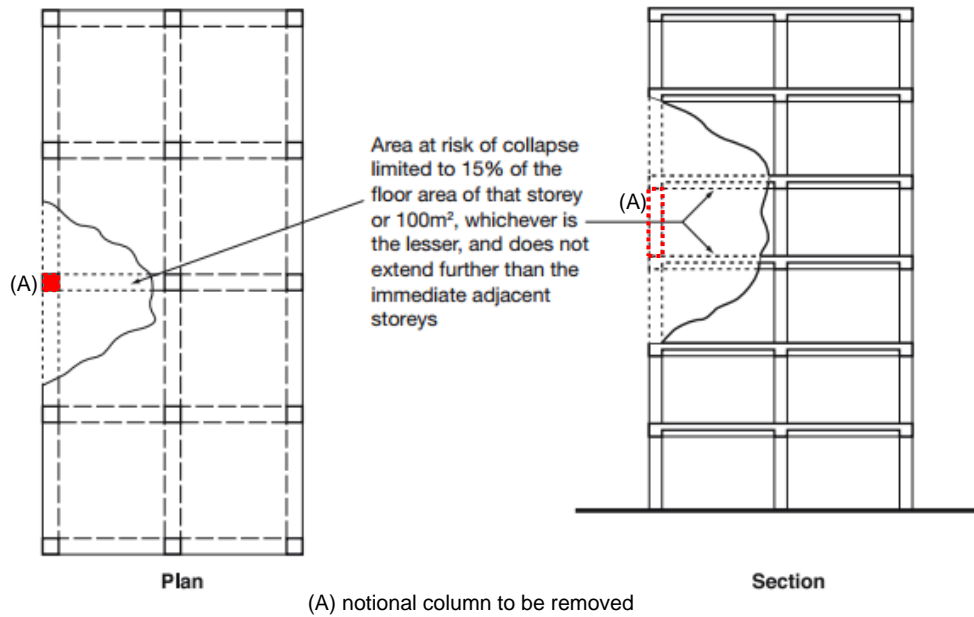
Fig. 2.3. Damage extension - adapted from [79]

2.4 Artificially Accounting for the Presence of Stirrups and Confinement Effect

Concrete strength is a determinant factor in high building and/or seismic designed RC structures. The use of high strength concrete in these cases is justified since it usually results in smaller cross sectional areas and, therefore, lower self-weight loads. However, high strength concrete tends to present lower ductility when compared to general-use concrete, as explained by HUSEM and PUL [80]. Many authors have addressed the relationship between the transverse reinforcement ratio and the improvement of concrete properties as maximum compressive strength and ductility. The recent work of ELKOLY and EL-ARISS [66] in the PC field applies a multiplying factor of 1.2 to scale up concrete stress-strain relationship. In this work, the same value is used to artificially account for the presence of stirrups and their confinement effect on concrete compressive strength. The following works support this choice.

HUSEM and PUL [80] present the results of testing 36 prismatic RC specimens. The specimens were reinforced in both directions (longitudinal and transversal) in order to investigate how the arrangement of those reinforcements influences concrete strength and ductility. The findings show that these properties are lowered by the increasing of the distance between the steel transverse reinforcement bars (confinement effect). In the other hand, concrete strength was up to 19% higher when this distance was shortened.

The results of HUSEM and PUL [80] are in agreement with MANDER *et al.* [81], who proposed a stress-strain model for predicting the behavior of uniaxially loaded

RC specimens with different shapes and reinforcement schemes. The effects of cyclic loading is taken into account, as well as the effects of the rate of change in strain with respect to the time (also known as strain-rate effects). Examples provided by MANDER *et al.* [81] show how concrete compressive strength increases with more than 16.0% in monotonically loaded specimens. Meanwhile, when strain-rates are considered, the model provides an increase of 27.0% for the concrete compressive strength and initial stiffness, and a reduction of 13.0% in the value of strain related to the maximum compressive stress. The results obtained with the theoretical model reflected the ones presented in MANDER *et al.* [81]. The authors point out how different confinement scenarios contribute to the strengthening of concrete. The better performance of circular columns over rectangular and squared ones is analytically predicted and experimentally proven by the authors.

Effects of concrete confinement are also present when using welded reinforcement grids as transverse reinforcement. This improvement is demonstrated by the experimental results of SAATCIOGLU and GRIRA [82]. Different configurations were chosen for the grids (4 and 9 cells) and for the longitudinal reinforcement (4, 8, 12 and 20 bars) welded together. The authors report the higher deformability of columns with 9-cell grids and similar behavior of the columns when the position of the longitudinal bars is varied. Last, the authors present welded grids as a faster and economic alternative to be employed in the construction of seismic structures.

However, increasing the transverse reinforcement ratio is not always the solution for obtaining more ductile and stronger RC elements. HO *et al.* [83] analytically demonstrated that concrete confinement has beneficial impact on enhancing the flexural ductility of columns but also demonstrated that this enhancement decreases for higher strength concretes or in the presence of high axial load levels. These results are in agreement with the numerical ones from BHOWMICK *et al.* [84]. Some other results from BHOWMICK *et al.* [84] were: the confinement is more effective with grids as transverse reinforcements, bettering the performance of columns as the number of grid cells increases; the distribution of longitudinal reinforcement also contributes to confining the concrete; as in the experiments of MANDER *et al.* [81], circular columns present better performance.

Table 2.1
Consequence classes and recommended approaches

Class	Example*	Recommended approach
CC1	single occupancy houses not exceeding 4 storeys	no specific consideration except to ensure stability and minimum robustness
CC2 - lower risk	hotels not exceeding 4 storeys	provision of horizontal ties for framed constructions (simplified analysis by static equivalent models)
CC2 - upper risk	hotels greater than 4 storeys but not exceeding 15 storeys	provision of horizontal and vertical ties, or alternatively, verification of stability and local damage extension upon the notional removal of each supporting column and each beam supporting a column (simplified analysis by static equivalent models)
CC3	all buildings that exceed the limits of storeys covered by CC2	systematic risk assessment considering both foreseeable and unforeseeable hazards (dynamic analyses, nonlinear models and the interaction between loads and structure may be required)

* see EUROCODE [78], for additional examples

23

Chapter 3

Computational Developments

The formulations proposed herein are applicable for plane frames and couple a multiscale computation of sectional stresses (IRIBARREN [63]) to geometrically nonlinear kinematics, based on a corotational Bernoulli beam formulation. The derivation of the internal force vector and structural stiffness matrix, necessary to solve the nonlinear problem using a Newton-Raphson scheme[1], is presented in the following.

The multilayered discretization of the element's cross section is described, as well as the return mapping for the plastic problem and the dynamic integration procedures. The adopted material stress-strain relationships at the level of constituents and the inclusion of the strain rate effects[2] are also discussed.

3.1   Corotational Beam Formulation

In a corotational formulation, strains and stresses are obtained in an individual reference system (x, z) attached to the beam element (Fig. 3.1), instead of in a global, structural reference system (X, Z). This approach allows decoupling the rigid body rotation from the beam deformation in a natural way. Similar developments of geometrically nonlinear beam formulations were used in BATTINI [35], with a different cross sectional stress integration scheme for mono-material steel beams. Another similar formulation can be found in CRISFIELD [34], who assumed linear material behavior and a different local displacement definition.

---

[1] Partially developed during the participation of the reseacher on the Programa de Doutoramento Sanduíche no Exterior, at the Université Libre de Bruxelles, in Brussels/Belgium.
[2] Previously developed by IRIBARREN [63]
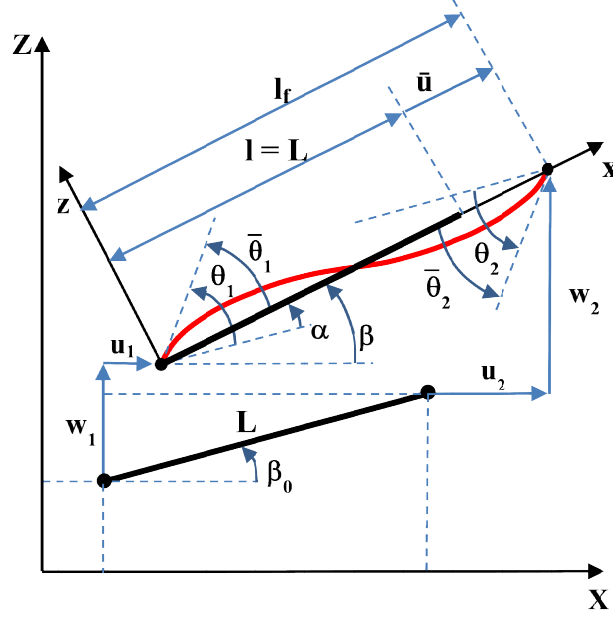
Fig. 3.1. Corotational reference system and kinematic variables

The displacement components in the global reference system and in the local reference system can be identified on Fig. 3.1 and are given by:

$$\mathbf{q}_{global}^{T} = \left\{ u_1 \quad w_1 \quad \theta_1 \quad u_2 \quad w_2 \quad \theta_2 \right\} \tag{3.1}$$

$$\mathbf{q}_{local}^{T} = \left\{ \bar{u} \quad \bar{\theta}_1 \quad \bar{\theta}_2 \right\} \tag{3.2}$$

In the same figure, the angles α, β, β_0 denote respectively the rigid body rotation of the element, the current angle between the element and the global reference system, and the original value of this angle in the undeformed configuration. In the corotational system, the element axial displacement and the rotations are denoted by $\bar{u}$, $\bar{\theta}_1$ and $\bar{\theta}_2$, respectively. The nodal coordinates of the element in the global reference system are denoted by (X_1, Z_1) and (X_2, Z_2) and the following relations can be derived for β_0 and β in terms of nodal coordinates and displacements:

$$c_o = \cos \ \beta_o = \frac{1}{L}(X_2 - X_1) \tag{3.3a}$$

$$s_o = \sin \ \beta_o = \frac{1}{L}(Z_2 - Z_1) \tag{3.3b}$$

$$c = \cos \ \beta = \frac{1}{l_f}(X_2 - X_1 + u_2 - u_1) \tag{3.3c}$$

$$s = \sin \ \beta = \frac{1}{l_f}(Z_2 - Z_1 + w_2 - w_1) \tag{3.3d}$$

where L and l_f are the undeformed and the deformed element lengths. These

relations define the rigid body rotation angle by:

$$\alpha = \beta - \beta_0 \tag{3.4}$$

The following trigonometric relationships are valid:

$$\sin \alpha = c_o s - s_o c \tag{3.5a}$$

$$\cos \alpha = c_o c - s_o s \tag{3.5b}$$

From the beam length change and the angles β_0 and β, the displacements in the local frame are computed as:

$$\begin{bmatrix} \bar{u} \\ \bar{\theta}_1 \\ \bar{\theta}_2 \end{bmatrix} = \begin{bmatrix} l_f - L \\ \theta_1 - \alpha \\ \theta_2 - \alpha \end{bmatrix} = \begin{bmatrix} l_f - l \\ \theta_1 - \beta - \beta_0 \\ \theta_2 - \beta - \beta_0 \end{bmatrix} \tag{3.6}$$

The local displacement vector obtained in Eq. 3.6 is energetically conjugated to the following local internal force vector:

$$\mathbf{f}_{local,\text{int}} = \left\{ \bar{N} \quad \bar{M}_1 \quad \bar{M}_2 \right\}^T \tag{3.7}$$

where the normal force $\bar{N}$ is constant along the length of the element, while the moments $\bar{M}_1$ and $\bar{M}_2$ are applied to the nodes (1 and 2), respectively.

The global internal force vector, associated to the global displacements, is given as a function of the local internal force vector:

$$\left\{ f_1^X \quad f_1^Z \quad c_1 \quad f_2^X \quad f_2^Z \quad c_2 \right\}^T = \mathbf{T}^T \left\{ \bar{N} \quad \bar{M}_1 \quad \bar{M}_2 \right\}^T \tag{3.8}$$

where the indexes $(1, 2)$ denote the node numbers. The derivation of this transformation matrix ($\mathbf{T}$) is quite simple (CRISFIELD [34], BATTINI [35]) and gives:

$$\mathbf{T} = \begin{bmatrix} 1 & 1/l_f & 1/l_f \end{bmatrix} \begin{bmatrix} -c & -s & 0 & c & s & 0 \\ s & -c & 1 & s & c & 0 \\ s & -c & 0 & s & c & 1 \end{bmatrix} \tag{3.9}$$

In order to use a Newton-Raphson procedure for solving the structural equilibrium problem, the consistent tangent stiffness matrix ($\mathbf{K}$) of the beam finite element is required. This matrix is defined as the derivative of the global internal forces with

respect to the variation of the global displacements:

$$\delta\mathbf{f}_{global,\text{int}} = \delta\left(\mathbf{T}^T\mathbf{f}_{local,\text{int}}\right)$$
$$= \mathbf{T}^T\delta\mathbf{f}_{local,\text{int}} + \bar{N}\delta\mathbf{t}_1 + \bar{M}_1\delta\mathbf{t}_2 + \bar{M}_2\delta\mathbf{t}_3 \tag{3.10}$$

where $\mathbf{t}_j$ is the $j-th$ row of the transformation matrix $\mathbf{T}$.

Differentiation of the $\mathbf{t}_j$-vectors yields:

$$\delta\mathbf{t}_1 = \delta\mathbf{r} \tag{3.11a}$$

$$\delta\mathbf{t}_2 = \delta\mathbf{t}_3 = -\frac{\delta\mathbf{z}}{l_f} + \frac{\mathbf{z}\delta l_f}{l_f^2} \tag{3.11b}$$

where the quantity δl_f and the auxiliary vectors $\delta\mathbf{r}$ and $\delta\mathbf{z}$ are given by

$$\delta l_f = \begin{bmatrix} -c & -s & 0 & c & s & 0 \end{bmatrix}^T \delta\mathbf{q}_{global} \tag{3.12a}$$

$$\delta\mathbf{r} = \begin{bmatrix} s & -c & 0 & -s & c & 0 \end{bmatrix}^T \delta\beta \tag{3.12b}$$

$$\delta\mathbf{z} = -\begin{bmatrix} -c & -s & 0 & c & s & 0 \end{bmatrix}^T \delta\beta \tag{3.12c}$$

The angle β is obtained from Eqs. 3.3 and the quantity $\delta\beta$ can be represented as:

$$\delta\beta = \frac{\mathbf{z}^T}{l_f}\delta\mathbf{q}_{global} \tag{3.13}$$

Substituting now the Eq. 3.13 into Eqs. 3.12 and applying the result to Eqs. 3.11 yields:

$$\delta\mathbf{t}_1 = \frac{\mathbf{z}\mathbf{z}^T}{l_f}\delta\mathbf{q}_{global} \tag{3.14a}$$

$$\delta\mathbf{t}_2 = \delta\mathbf{t}_3 = \frac{1}{l_f^2}\left(\mathbf{r}\mathbf{z}^T + \mathbf{z}\mathbf{r}^T\right)\delta\mathbf{q}_{global} \tag{3.14b}$$

where

$$\mathbf{r} = \begin{bmatrix} -c & -s & 0 & c & s & 0 \end{bmatrix}^T \tag{3.15a}$$

$$\mathbf{z} = \begin{bmatrix} s & -c & 0 & -s & c & 0 \end{bmatrix}^T \tag{3.15b}$$

Substituting Eqs. 3.14 into Eq. 3.10 gives:

$$\delta \mathbf{f}_{global,\text{int}} = \mathbf{T}^T \delta \mathbf{f}_{local,\text{int}} + \left[\bar{N} \frac{\mathbf{z}\mathbf{z}^T}{l_f} + \left(\bar{M}_1 + \bar{M}_2 \right) \frac{1}{l_f^2} \left(\mathbf{r}\mathbf{z}^T + \mathbf{z}\mathbf{r}^T \right) \right] \delta \mathbf{q}_{global} \quad (3.16)$$

The first term on the right hand side of Eq. 3.16 is given by:

$$\mathbf{T}^T \delta \mathbf{f}_{local,\text{int}} = \mathbf{T}^T \mathbf{K}_{local} \delta \mathbf{q}_{local} = \mathbf{T}^T \mathbf{K}_{local} (\mathbf{T} \delta \mathbf{q}_{global}) \quad (3.17)$$

The matrix $\mathbf{K}_{local}$ is introduced as the local stiffness matrix and only depends on the material constitutive properties and the initial geometrical characteristics. The derivation of $\mathbf{K}_{local}$ is discussed in the next sections.

The differentiation of the global internal force vector can finally be expressed as:

$$\delta \mathbf{f}_{global,\text{int}} = \left[\mathbf{T}^T \mathbf{K}_{local} \mathbf{T} + \bar{N} \frac{\mathbf{z}\mathbf{z}^T}{l_f} + \left(\bar{M}_1 + \bar{M}_2 \right) \frac{1}{l_f^2} \left(\mathbf{r}\mathbf{z}^T + \mathbf{z}\mathbf{r}^T \right) \right] \delta \mathbf{q}_{global} \quad (3.18)$$

which defines the global consistent stiffness matrix ($\mathbf{K}_{global}$) as

$$\mathbf{K}_{global} = \underbrace{\mathbf{T}^T \mathbf{K}_{local} \mathbf{T}}_{K_M} + \underbrace{\bar{N} \frac{\mathbf{z}\mathbf{z}^T}{l_f} + \left(\bar{M}_1 + \bar{M}_2 \right) \frac{1}{l_f^2} \left(\mathbf{r}\mathbf{z}^T + \mathbf{z}\mathbf{r}^T \right)}_{K_G} \quad (3.19)$$

where K_M is associated to the changes to the material while K_G relates to the geometry changes.

3.2   Corotational Multilayered Bernoulli Beam Element

The Bernoulli beam element is based on the classical assumption that plane sections remain plane and normal to the longitudinal axis after deformation. Three Gauss points distributed along the length of the element define reference sections as in IRIBARREN [63]. These sections are discretized in a finite number of layers which, on their turn, are used in a finite summation for obtaining the local internal force vector ($\mathbf{f}_{local,\text{int}}$) and the local stiffness matrix ($\mathbf{K}_{local}$).

3.2.1   Local displacement interpolation and strain components

For this element, the axial (u_{local}) and vertical (w_{local}) displacements are interpolated along its length in the corotated system of coordinates (x, z), using linear and cubic

shape functions (BATTINI [35]), respectively:

$$u_{local} = \frac{x}{l}\bar{u} \tag{3.20a}$$

$$w_{local} = x\left(1 - \frac{x}{l}\right)^2\bar{\theta}_1 + \frac{x^2}{l}\left(\frac{x}{l} - 1\right)\bar{\theta}_2 \tag{3.20b}$$

The axial strain ($\bar{\varepsilon}$) and curvature (χ) are obtained by derivation of Eqs. 3.20 and are recast in the vector of generalized strains:

$$\mathbf{E}^{gen} = \begin{bmatrix} \bar{\varepsilon} \\ \chi \end{bmatrix} = \begin{bmatrix} \frac{\partial u_{local}}{\partial x} \\ \frac{\partial^2 w_{local}}{\partial x^2} \end{bmatrix} \tag{3.21}$$

Based on these relationships, the total axial strain (ε) at a given beam depth (z) of a section at the longitudinal position x (Fig. 3.2), is equal to:

$$\varepsilon(x,z) = \frac{\partial u_{local}}{\partial x} - \chi z = \frac{\bar{u}}{l} - z\left[\left(6\frac{x}{l^2} - \frac{4}{l}\right)\bar{\theta}_1 + \left(6\frac{x}{l^2} - \frac{2}{l}\right)\bar{\theta}_2\right] \tag{3.22}$$
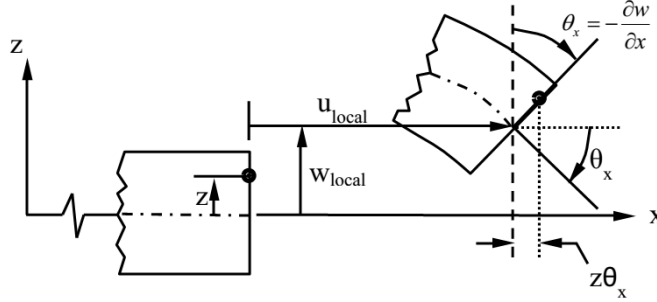
Fig. 3.2. Displacements of a Bernoulli beam

3.2.2 The local internal force vector

The distribution of the total axial strain ($\varepsilon(z)$) on the element cross sectional area (a_{cor}), at a fixed axial position (x) in the corotated axes, is work-conjugate to the one-dimensional normal stress distribution ($\sigma(z)$). This normal stress is used for obtaining the stress resultants in the section at a given axial position x, as follows:

$$N = \int_{a_{cor}} \sigma\,da \tag{3.23a}$$

$$M = -\int_{a_{cor}} \sigma z\,da \tag{3.23b}$$

29

where, N is the normal force, M is the bending moment and z is the vertical distance of a point with respect to the cross sectional gravity center (Fig. 3.3). Given the layer strains, a multilayer approach is used to compute the stress resultants, as will be explained in details in the next section.

Fig. 3.3. Sectional bending moment and normal force

The internal work can be expressed as an integral over the element volume in the corotated local axes (v_{cor}):

$$W_{\text{int}} = \int\limits_{v_{cor}} \sigma \, \delta\varepsilon \, dv \tag{3.24}$$

which, after introducing Eq. 3.22, becomes

$$W_{\text{int}} = \int\limits_{v_{cor}} \sigma \left\{ \frac{\delta\bar{u}}{l} - z \left[\left(6\frac{x}{l^2} - \frac{4}{l} \right) \delta\bar{\theta}_1 + \left(6\frac{x}{l^2} - \frac{2}{l} \right) \delta\bar{\theta}_2 \right] \right\} dv \tag{3.25}$$
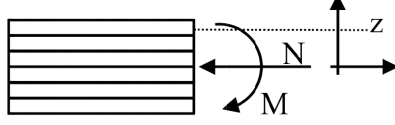
Equation 3.25 is valid for all sets of $\left(\delta\bar{u}, \delta\bar{\theta}_1, \delta\bar{\theta}_2 \right)$. Thus, the conjugated internal forces read:

$$\bar{N} = \int\limits_{v_{cor}} \frac{\sigma}{l} \, dv = \int\limits_{l} \frac{N}{l} \, dl \tag{3.26a}$$

$$\bar{M}_1 = - \int\limits_{v_{cor}} \sigma z \left(6\frac{x}{l^2} - \frac{4}{l} \right) dv = \int\limits_{l} M \left(6\frac{x}{l^2} - \frac{4}{l} \right) dl \tag{3.26b}$$

$$\bar{M}_2 = - \int\limits_{v_{cor}} \sigma z \left(6\frac{x}{l^2} - \frac{2}{l} \right) dv = \int\limits_{l} M \left(6\frac{x}{l^2} - \frac{2}{l} \right) dl \tag{3.26c}$$

to which a Gauss numerical integration scheme is applied, using three integration points along the beam length.

3.2.3 The multilayered approach

To derive the material response, it is necessary to numerically determine the stress resultants N and M. Thus, the cross sectional area is divided in a finite number of *perfectly bonded* longitudinal layers (Fig. 3.4) for the evaluation of strains and stresses in the section. The same approach is used in IRIBARREN [63], in a geometrically linear scenario, including material nonlinearities and viscoplastic effects.

Considering classical linear Bernoulli beam kinematics, the shear effects are not taken into account and the transverse reinforcement is disregarded.
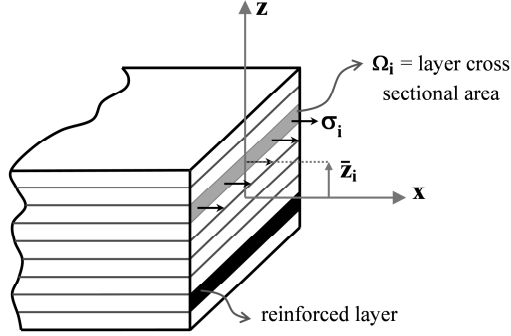

Fig. 3.4. Multilayer discretization of a Bernoulli beam section

For a given layer i, the total axial strain at a fixed axial position x (Eq. 3.22) is given by:

$$\varepsilon_i = \frac{\partial u}{\partial x} - \chi \bar{z}_i = \frac{\bar{u}}{l} - \bar{z}_i \left[\left(6\frac{x}{l^2} - \frac{4}{l} \right) \bar{\theta}_1 + \left(6\frac{x}{l^2} - \frac{2}{l} \right) \bar{\theta}_2 \right] \qquad (3.27)$$

where $\bar{z}_i$ is the position of the layer's cross sectional gravity center with respect to the gravity center of the whole cross section (Fig. 3.4); For the sake of simplicity, the axial displacement u_{local} will, from this point on, be represented as u.

The total axial strain value of a given layer allows determining the one-dimensional normal stress acting in this layer via nonlinear one-dimensional constitutive relationships for concrete and steel, $\sigma_{i,conc}(\varepsilon_i)$ and $\sigma_{i,steel}(\varepsilon_i)$, which are presented in Section 3.2.5. As already mentioned, perfect bonding is assumed for the interface between steel and concrete and a mixture rule is used for obtaining stresses on composite layers containing both materials. Therefore, the composite layer's normal stress $(\sigma_{i,total})$ is given by:

$$\sigma_{i,total} = \frac{\Omega_i - \Omega_{i,steel}}{\Omega_i} \sigma_{i,conc} + \frac{\Omega_{i,steel}}{\Omega_i} \sigma_{i,steel} \qquad (3.28)$$

where Ω_i is the total cross sectional area of the layer i and $\Omega_{i,steel}$ is the area of steel in this layer.

Having $\sigma_{i,total}$ calculated for all layers of the section, the integrals that provide the stress resultants (Eqs. 3.26) are evaluated as sums of the contributions of each layer, $i.e.$:

$$N = \sum_i \sigma_{i,total} \Omega_i \qquad (3.29a)$$

$$M = \sum_i -\bar{z}_i \sigma_{i,total} \Omega_i \qquad (3.29b)$$

31

3.2.4   The local stiffness matrix

A consistent tangent operator for each layer can be defined as:

$$H_i = \frac{\partial \sigma_{i,total}}{\partial \varepsilon_i} \tag{3.30}$$

Based on the layers' response, the consistent tangent operator on the sectional level ($\mathbf{H}$) is computed as follows:

$$\mathbf{H} = \frac{\partial \mathbf{\Sigma}^{gen}}{\partial \mathbf{E}^{gen}} = \begin{bmatrix} \sum_i H_i \Omega_i & -\sum_i H_i \bar{z}_i \Omega_i \\ -\sum_i H_i \bar{z}_i \Omega_i & -\sum_i H_i \bar{z}_i^2 \Omega_i \end{bmatrix} \tag{3.31}$$

where $\mathbf{\Sigma}^{gen} = \begin{bmatrix} N & M \end{bmatrix}^T$ is the vector of stress resultants and $\partial \mathbf{E}^{gen}$ is given by Eq. 3.21.

The local stiffness matrix ($\mathbf{K}_{local}$) can be obtained in a standard way as:

$$\mathbf{K}_{local} = \int_l \mathbf{B}^T \mathbf{H} \mathbf{B} \, dl \tag{3.32}$$

where $\mathbf{H}$ is the consistent tangent operator on the sectional level (Eq. 3.31) and $\mathbf{B}$ is the matrix of the derivatives of the local shape functions (Eqs. 3.20) given by:

$$\mathbf{B} = \begin{bmatrix} \frac{1}{l} & 0 & 0 \\ 0 & \left(6\frac{x}{l^2} - \frac{4}{l}\right) & \left(6\frac{x}{l^2} - \frac{2}{l}\right) \end{bmatrix} \tag{3.33}$$

Note that, considering the classical linear Bernoulli beam assumptions in the corotational system of coordinates, $\mathbf{K}_{local}$ only depends on the material constitutive properties and the initial geometrical characteristics.

3.2.5   Constitutive behavior of steel and concrete

Within the multilayered beam formulation, for the Bernoulli beam element, the stress-strain relationship of the constituents is described through simplified models. These approximations are in accordance with EUROCODE [37] and *fib* [38, 39], and provide the data that are directly used in the computational model.

The following assumptions are used for describing the material behavior of concrete and steel (Figs. 3.5 and 3.6):
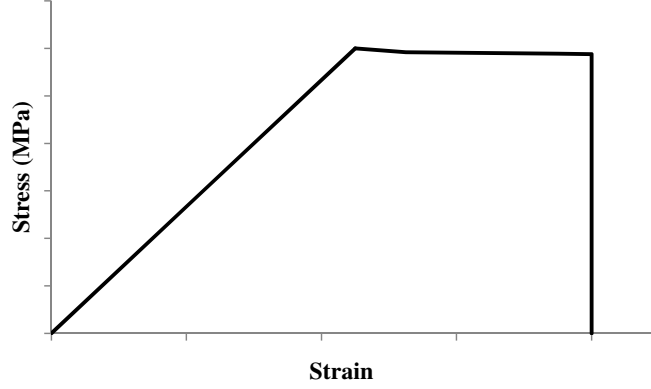
Fig. 3.5. Quasi-static concrete behavior for the Bernoulli beam element

- perfect bonding between the materials is assumed, *i.e* debonding is not taken into account;

- any structural strength associated with concrete tensile loading is not taken into account, *i.e.*, concrete under tension is considered to be fully cracked and the corresponding tensile stresses are neglected;

- instead of the nonlinear curve proposed by *fib* [38, 39], the adopted model uses proportionality between strains and stresses in the elastic regime, as recommended by EUROCODE [37];

- as in IRIBARREN [63], for quasi-static loading conditions, the concrete behavior during the plastic regime is governed by the following softening law:

$$\sigma_{h,conc} = \sigma_{0,conc} \exp\left(\mu \kappa_{conc}\right) \tag{3.34}$$

where $\sigma_{h,conc}$ is the current maximum compressive stress, $\sigma_{0,conc}$ is the initial maximum compressive stress, μ is a softening parameter and κ_{conc} is the cumulated plastic strain in concrete;

- the steel behavior in tension is analogous to the one in compression, and the *buckling* of compressed steel bars is *not taken into account*. As in IRIBARREN [63], the plastic behavior of steel is represented by the following hardening law:

$$\sigma_{h,steel} = \sigma_{0,steel}\left(1 + \eta \kappa_{steel}\right) \tag{3.35}$$

where $\sigma_{h,steel}$ is the current yield limit, $\sigma_{0,steel}$ is the initial yield stress, η is a hardening parameter and κ_{steel} is the cumulated plastic strain in steel;
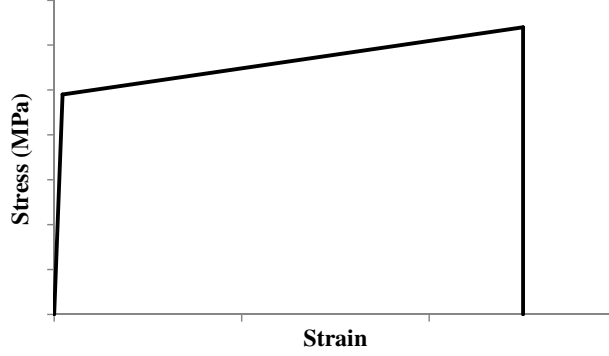
Fig. 3.6. Quasi-static steel behavior for the Bernoulli beam element

- when reaching the ultimate strain under compression, any increase in the strain level will immediately decrease the stress to zero and keep it at this level in the subsequent loading steps. In this work, this assumption associated with the multilayer discretization allows representing the progressive material degradation due to compressive concrete failure (crushing);

- stresses in the layers vanish if the strain values are larger than the ultimate strain whether in tension or compression, representing steel fracture.

3.2.6   Strain rate and dynamic effects

Since progressive collapse (PC) is a dynamic phenomenon, a dynamic framework is used to describe the structural equilibrium in the numerical model[3]. Equilibrium in structural dynamics is represented by the following equation:

$$\mathbf{f}_{int}\left(\mathbf{q}, \dot{\mathbf{q}}\right) + \mathbf{M}\ddot{\mathbf{q}} = \mathbf{f}_{ext} \tag{3.36}$$

on which an implicit Newmark integration scheme is applied and where $\mathbf{f}_{int}$ represents the internal force vector, dependent on the displacements $\mathbf{q}$ and the displacements rates $\dot{\mathbf{q}}$. The mass matrix is represented by $\mathbf{M}$, $\ddot{\mathbf{q}}$ is the vector of nodal accelerations and $\mathbf{f}_{ext}$ is the external force vector. Note that no numerical/artificial damping is introduced in the system of equations.

The internal forces are strain rate dependent and their variation with respect to the displacements, *i.e.*, the structural tangent operator, is also dependent on those rates. This dependency introduces, therefore, a viscous damping term:

$$\mathbf{K}_T = \left.\frac{\partial \mathbf{f}_{int}\left(\mathbf{q}, \dot{\mathbf{q}}\right)}{\partial \mathbf{q}}\right|_{\dot{\mathbf{q}}=cte} + \left.\frac{\partial \mathbf{f}_{int}\left(\mathbf{q}, \dot{\mathbf{q}}\right)}{\partial \dot{\mathbf{q}}}\right|_{\mathbf{q}=cte} \frac{\partial \dot{\mathbf{q}}}{\partial \mathbf{q}} \tag{3.37}$$

---

[3]Previously developed by IRIBARREN [63]

34

where the second term on the right side introduces damping at the structural level due to the strain rate dependent (viscoplastic) stress-strain relationships assumed for the materials.

It should be noted that the mass matrix of the beam elements was here calculated considering the undeformed shape of the structure and kept constant along the entire analysis in this work.

In order to account for the strength enhancement provided by the strain rate dependence of both steel and concrete material behavior (BISCHOFF and PERRY [85] and MALVAR and CRAWFORD [86]), the constitutive models defined in Section 3.2.5 are extended by a strain rate dependent material behavior. The elastic modulus of concrete is therefore made dependent on the strain rate (see IRIBARREN [63] and IRIBARREN *et al.* [36] for more details). Moreover, to include the strain rate effects in the irreversible behavior of concrete and steel, a Perzyna type viscoplastic model is used (HEERES *et al.* [87]), introducing viscous terms in the constitutive laws.

The viscoplastic strain rate is a function of the overstress value and is given as follows:

$$\dot{\varepsilon}^{vp} = \frac{1}{\lambda} \left\langle \frac{f}{\sigma_{0,mat}} \right\rangle^n \frac{df}{d\sigma} \tag{3.38}$$

where $\langle ... \rangle$ are called MacAulay brackets, $\dot{\varepsilon}^{vp}$ is the viscoplastic strain rate, $\sigma_{0,mat}$ is the material (steel or concrete) initial yield/maximum compressive stress; and λ and n are viscosity parameters. The parameter λ depends on the strain rate and $N = 1$, as assumed by IRIBARREN [63] and IRIBARREN *et al.* [36] in order to obtain a good agreement with the experimental results of MALVAR and CRAWFORD [86]. The overstress function(f) is given by ($\sigma_{mat} - \bar{\sigma}_{mat}$) , where σ_{mat} is the one-dimensional stress, for steel or concrete, and $\bar{\sigma}_{mat}$ is the current yield stress/maximum compressive stress.

Chapter 4

Quasi-Static Analysis of Monotonically Loaded Planar Frames

This chapter establishes a direct correlation between experimental results available on the literature and the ones obtained in a numerical analysis using the herein developed Bernoulli finite element. The numerical assessment of the failure response of two reinforced concrete(RC) structures (LEW *et al.* [32], YI *et al.* [33]) is investigated in order to address the mechanism of Progressive Collapse (PC)[1]. These structures were selected within a significant body of literature of experimental tests. The selection was made considering: (*i*) the amount of available information on the experimental conditions that would allow the direct numerical representation of the laboratory conditions (geometry, constituent material parameters, loading pattern, etc.); (*ii*) the available information on the experimental structural response, in which different failure mechanisms and the sequence of their appearance had been clearly identified.

The following organization is used: first, the frame models used to simulate the chosen experiments are presented; second, the material behavior for concrete and steel is defined based on the available experimental data (LEW *et al.* [32], YI *et al.* [33]). Then the obtained numerical results are presented and compared to the experimental ones from the literature. Variation of several material parameters for both structures are also reported and discussed. Finally, a general discussion on the results is given.

4.1 Intermediate Moment Frame (IMF)

LEW *et al.* [32] (also SADEK *et al.* [46]) experimentally investigated the behavior of a reinforced concrete beam-column assemblage subjected to column failure. This

---

[1]Partially developed during the participation of the researcher on the Programa de Doutoramento Sanduíche no Exterior, at the Université Libre de Bruxelles, in Brussels/Belgium.

structure represents a portion of a ten-story RC frame building and was designed for seismic category C as an intermediate moment frame (IMF) according to the ACI [88] requirements.

4.1.1 Experimental setup and numerical model

The structural assemblage consists of two beams of section 711×508 mm supported by three columns of section 711×711 mm (Fig. 4.1). The exterior columns were fully restrained at the bottom. Only the horizontal movement of these columns was blocked at the top, allowing vertical motion and rotations. Meanwhile, the middle column was just partially built between the two beams. Progressive structural failure resulting from the lack of the middle column support was simulated by the application of a monotonically increasing displacement at a rate of 25mm/min, which allows *quasi-static* numerical simulations. The dimensions of the structural members (beams and columns) and their respective longitudinal reinforcement schemes are shown on Fig. 4.1.
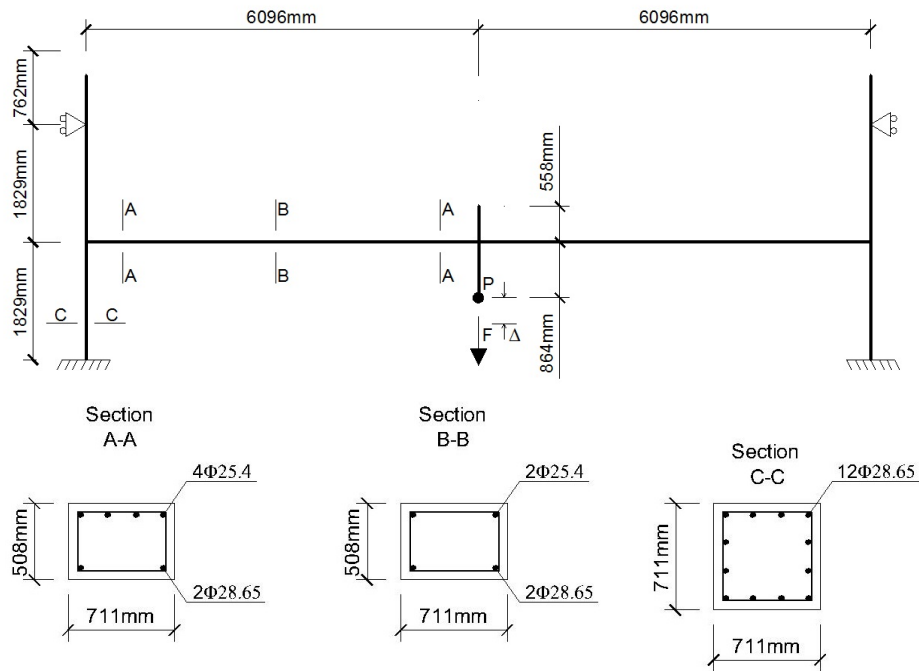

Fig. 4.1. IMF: schematic representation and reinforcement schemes, diameters given in millimeters

4.1.2 Experimentally measured material constitutive behavior

LEW *et al.* [32] previously tested cylinders ($\phi = 60$ mm, $h = 120$ mm) made of the same concrete used for building the IMF and obtained an experimental average com-

pressive strength (f_c^{exp}) of 32 MPa. During the PC experimental test, transducers were attached to the IMF obtaining relative displacements between target points. The relative displacement measurements were later used for determining concrete surface strain, for which the highest compressive value was calculated as 0.9%.

The longitudinal reinforcements consisted of ASTM A706 Grade 60 steel bars. The values shown in Tab. 4.1 were measured during the experiment of LEW *et al.* [32] and relate the steel yield strength $\sigma_{0,steel}$, ultimate strength $\sigma_{ult,steel}$ and highest strain $\varepsilon_{ult,steel}$ to the reinforcement bars diameter.

Table 4.1
Experimental data for steel reinforcement bars

Element	Diameter (mm)	$\sigma_{0,steel}$ (MPa)	$\sigma_{ult,steel}$ (MPa)	$\varepsilon_{ult,steel}$ (%)
Beam	25.40	476	648	21.0
Beam	28.65	462	641	18.0
Column	28.65	483	690	17.0

For the numerical representation of the structural model, steel and concrete material properties are considered to be the *same for beams and columns* and, for the sake of simplicity, the values of yield strength, ultimate strength and ultimate strain are herein defined as the average of the ones measured experimentally for the beams (Tab. 4.1), *i.e.*, $\sigma_{0,steel} = 469$ MPa, $\sigma_{ult,steel} = 645$ MPa and $\varepsilon_{ult,steel} = 19.5\%$, respectively. These values, applied to Eq. 3.35 define the linear hardening parameter value as $\eta = 1.95$. The steel Young modulus is equal to $E_{steel} = 200$ GPa, as recommend by EUROCODE [37]. Figure 4.2 depicts the stress-strain curve obtained with these values.
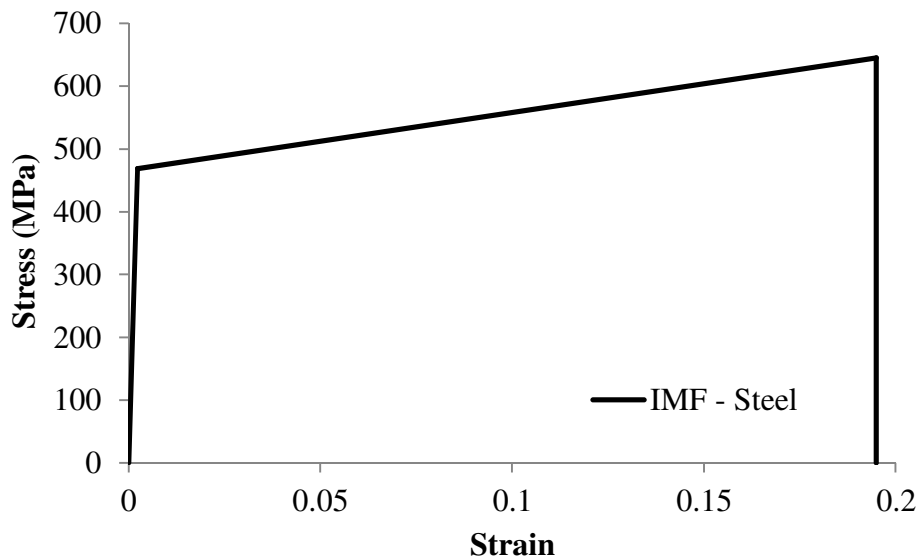

Fig. 4.2. Constitutive model - steel for quasi-static loading (IMF)

The concrete ultimate strain is considered to be equal to the highest value observed experimentally ($\varepsilon_{ult,conc} = 0.9\%$). In order to account for the effects of concrete confinement provided by stirrups, the maximum concrete compressive strength (f'_c) is considered to be approximately 20% higher than the measured experimental value, which gives $f'_c = 38$ MPa. This assumption is based on the results of MANDER *et al.* [81, 89]. The concrete Young modulus is calculated by using (f_c^{exp}) and the following equation, provided by ACI [88]:

$$E_{conc} = 4700\sqrt{f'_c} \tag{4.1}$$

which gives $E_{conc} = 27$ GPa.

In this work, concrete plastic behavior is an exponentially decreasing function (Eq.3.34) of the cumulated plastic strain (κ_{conc}). The softening parameter is here defined as $\mu = -5$, which provides a linear-like softening for the observed strain levels. This assumption of linearity complies with LEW *et al.* [32]. The resulting concrete constitutive behavior is shown on Fig. 4.3.
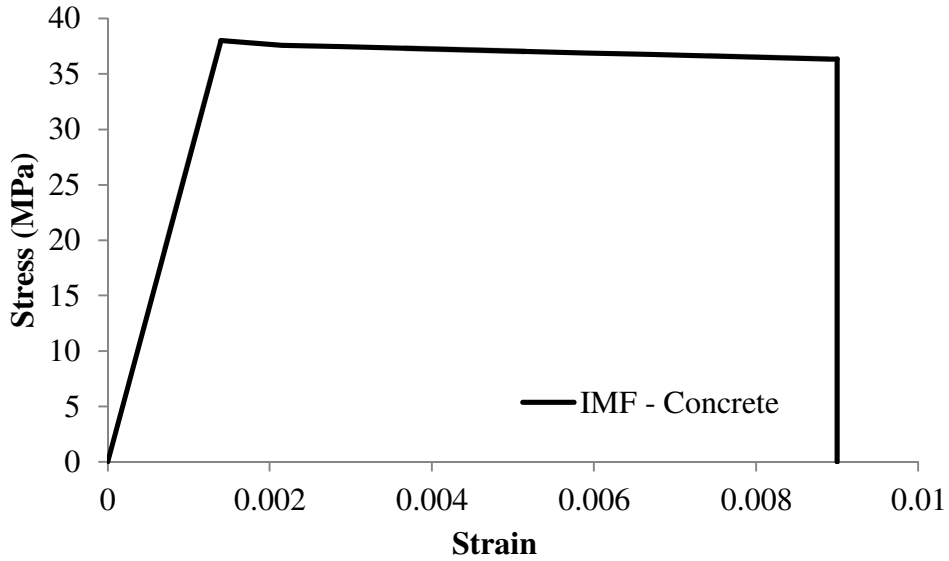
Fig. 4.3. Constitutive model - concrete for quasi-static loading (IMF)

Defining the set of material parameters that represent the structure in a numerical approach is a difficult task, mainly because of the dispersion of results in experimental tests. Parametric studies were performed in this work computationally to verify how changes in the material parameters affect the structural behavior of the selected models. A large number of authors have addressed the variability of the parameters that define concrete and steel constitutive behaviors. For instance, the concrete maximum compressive strength and ultimate strain is shown to depend on casting delay, pressure while concrete is in the fresh state, position/height on the structural element and, for reinforced concrete, the reinforcement arrange-

ment (SRI RAVINDRARAJAH [90], SCOTT *et al.* [91], TOOSSI [92], RANJBAR *et al.* [93]). Increasing of concrete maximum compressive strength (up to 115%) and ultimate strain (up to 570%) as function of the reinforcement schemes of differently shaped columns were reported by MANDER *et al.* [81, 89] when considering quasi-static analyses or loading at high strain rates. While studying steel samples produced by different mills, BOURNONVILLE *et al.* [94] observed large variations of the yield strength (413 to 588 MPa), tensile strength (551 to 799 MPa) and ultimate strain (14% to 21%). These values refer to ASTM A706 steel, the same type used as reinforcement of the IMF model analyzed in this work. Herein, the parametric studies consist in the individual variation of the maximum compressive strength and ultimate strain of concrete and ultimate strength and strain of steel, keeping all the other parameters at their reference values. Material parameters are taken as 80% and 120% of the values defined for the reference cases.

4.2 Three-story Scale Model (TSM)

The second selected structure was tested experimentally by YI *et al.* [33]. It represents the lower three stories of a four-bay, eight-story planar RC frame, designed in accordance with GB50010 [95], the Chinese design code for concrete structures. The tested structure is a one-third scale model and is depicted on Fig. 4.4.
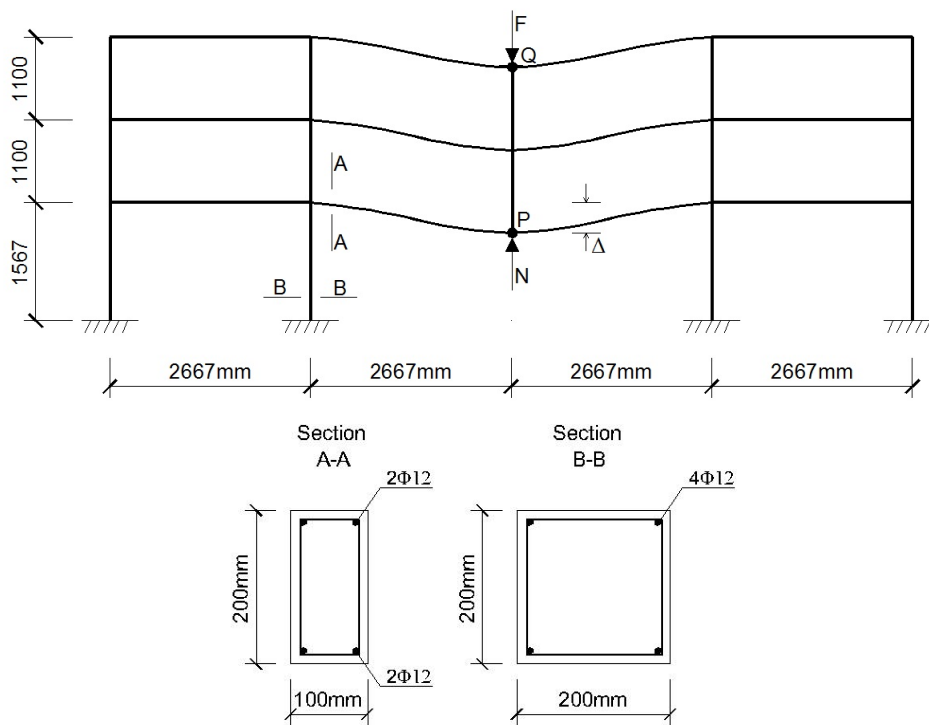

Fig. 4.4. TSM: schematic representation and reinforcement schemes, diameters given in millimeters

4.2.1 Experimental setup and numerical model

The planar frame consisted of four bays and three stories (Fig. 4.4). Each story height was of 1100 mm, except for the first one, which was 1567 mm high. The dimensions of the structural members (beams and columns) and their respective longitudinal reinforcement are also shown in Fig. 4.4.

A point load (F) was applied on the top of the middle column for simulating the gravity loads of the upper five stories. For simplicity, the gravity loads of the upper levels associated to the other columns were not incorporated in the experiment. The point load (N) represents the presence of the middle ground floor column that was not actually built. In the experiment of YI *et al.* [33], the Point (P) was connected to a load cell and two mechanical jacks that allowed adjusting the magnitude of the reaction force (N).

The modelling of the numerical loading sequence was based on YI *et al.* [33] and is reproduced here:

STEP 1 - the gravity loads of the stories between the application points P and Q (Fig. 4.4) were applied, causing deformation due to the self-weight;

STEP 2 - the vertical displacement of the Point P was constrained and the point force $F = 109.0$ kN was applied, accounting for the gravity loads above the third floor;

STEP 3 - after the application of F, the failure of the column was simulated by imposing a vertical displacement on point P.

4.2.2 Experimentally measured material constitutive behavior

Cubes ($15 \times 15 \times 15$ cm) made of concrete were tested by YI *et al.* [33] and the average compressive strength was measured as 25 MPa. During the experimental PC simulation, a value of 0.4% was measured as the highest concrete compressive strain. The values obtained in YI *et al.* [33] for steel yield strength and steel ultimate tensile strength were of 416 MPa and 526 MPa, respectively. Steel elongation was measured as 27.5% and 23.0% for 60 mm and 120 mm steel gauges, correspondingly.

Similar to the case of IMF, beams and columns are considered to have the same material properties in the numerical representation of the structural model. Accounting for the effects of concrete confinement (MANDER *et al.* [81, 89]), concrete compressive strength was assumed equal to $f_c' = 30$ MPa, *i.e.*, 1.2 times the value measured for the concrete cubes (YI *et al.* [33]). The concrete Young

modulus is calculated using the relation provided by Eq. 4.1 and is equal to $E_{conc} = 24$ GPa. The ultimate concrete strain was set to the experimentally measured value $\varepsilon_{ult,conc} = 0.4\%$ (YI *et al.* [33]). As in the previous analyses, the softening parameter of Eq. 3.34 is assumed $\mu = -5$, resulting in a linear-like descending slope of the stress-strain curve beyond the maximum compressive stress (Fig. 4.5).
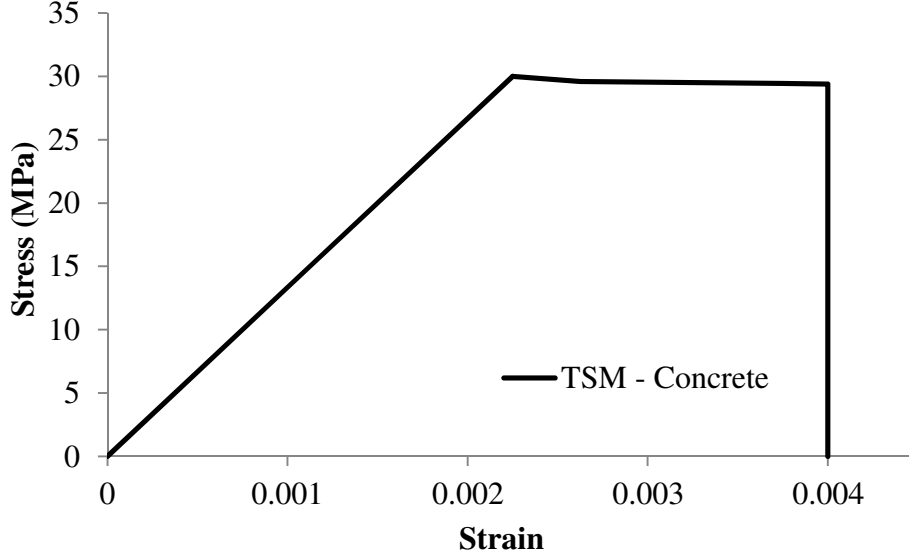

Fig. 4.5. Constitutive model - concrete for quasi-static loading (TSM)

A bilinear stress-strain relationship is adopted to represent steel constitutive behavior (Fig. 4.6). Steel Young modulus is equal to $E_{steel} = 200$ GPa, as recommend by EUROCODE [37]. The longitudinal reinforcement used by YI *et al.* [33] was composed of HRB400 steel bars. According to LIANQING *et al.* [96], the average values of yield strength, ultimate strength and ultimate strain, for HRB400 steel ($\phi = 12$ mm bars) are $\sigma_{0,steel} = 490$ MPa, $\sigma_{ult,steel} = 634$ MPa and $\varepsilon_{ult,steel} = 28\%$, respectively. These values define the hardening parameter of Eq. 3.35 as $\eta = 1.06$.

The properties of HRB400 steel, used for the TSM model, also display large variability in the material behavior. The minimum and maximum values of yield strength, tensile strength and elongation for different HRB400 bar diameters are $410 - 530$ MPa, $570 - 685$ MPa and $16 - 32\%$, according to LIANQING *et al.* [96]. By itself, this information justifies the need for parametric studies in order to investigate the influence of varying the material properties steel and can be extended to the studies of the concrete properties.

4.3 Computational Results

Computational FE models representing the two selected structures (LEW *et al.* [32], YI *et al.* [33]) were defined based on the geometries and material constitutive
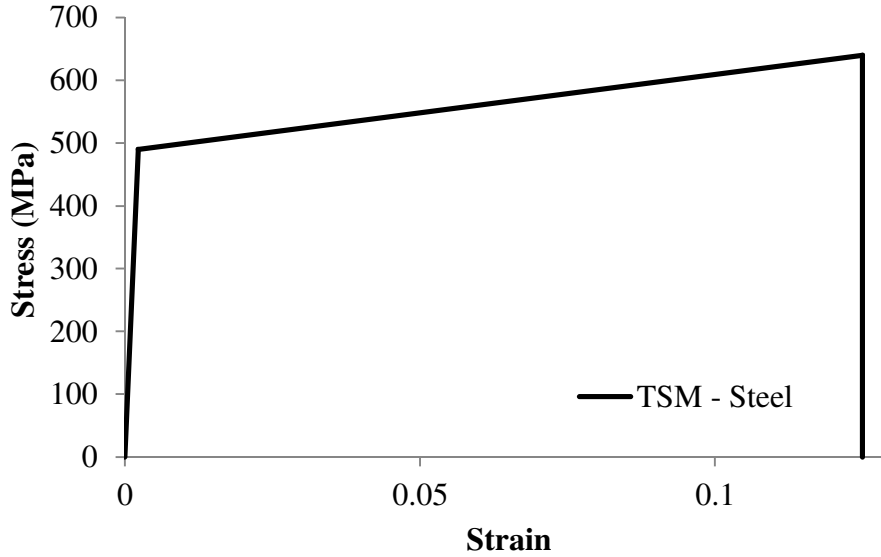
Fig. 4.6. Constitutive model - steel for quasi-static loading (TSM)

parameters previously presented. Those parameters and their respective models are referred in this section as *reference parameters* and *reference models*. The computational response of each structure is now presented in terms of load-displacement curves, pointing out specific features of the structural behavior, *i.e.*, the catenary effect, concrete crushing, steel yielding and reinforcement bar fracture, that are directly and explicitly traceable using the formulation presented in Chapter 3. They are compared to experimental results given in LEW *et al.* [32] and YI *et al.* [33].

4.3.1 Intermediate moment frame (IMF)

The reference load-displacement curve presented in Fig. 4.7 is obtained and is related to the deformed shapes of Fig. 4.8. Bold numbers in the text correspond to the ones measured during the experiment of LEW *et al.* [32] while numbers in regular characters were obtained computationally.

At an applied load of $240\,\mathrm{kN}/\mathbf{267}\,\mathrm{kN}$, the reinforcement bars in tension start yielding (P_1). The yielding occurs in structural sections $1 - 4$. The peak load of $317\,\mathrm{kN}/\mathbf{296}\,\mathrm{kN}$ is reached when the vertical displacement of the center column reaches $130\,\mathrm{mm}/\mathbf{127}\,\mathrm{mm}$ (P_2). After that, the load decreases with increasing displacement, which is associated with the crushing of concrete in structural sections 2 and 3. The load is stabilized at $155\,\mathrm{kN}/\mathbf{196}\,\mathrm{kN}$ at a displacement of $390\,\mathrm{mm}/\mathbf{406}\,\mathrm{mm}$ (P_3) and, with further increase in displacement, the load increases again due to catenary effects. The ultimate peak load of $531\,\mathrm{kN}/\mathbf{547}\,\mathrm{kN}$ is reached at the displacement of $1123\,\mathrm{mm}/\mathbf{1090}\,\mathrm{mm}$ (P_4). Note that this ultimate peak load corresponds to $2.25/\mathbf{2.04}$ times the first load peak. The final failure corresponds to the rupture of the bottom reinforcement bars of structural sections 2-3, causing a drop in load of a

43

magnitude of approximately half of the ultimate peak load. The numerical analysis was stopped at this point, since no further experimental data is available on the continuation of the curve (LEW *et al.* [32]).

A comparison between the numerical and experimental results (Fig. 4.7) shows that a very good agreement is obtained using the developed corotational beam element. The load values associated to the yielding of steel reinforcement bars and to the start of catenary effects are very similar, as well the peak loads. It is also particularly striking to observe that the sequence of events (*i.e.*, the successive degradation at different places in the structure) is also in accordance with the reported experimental data.
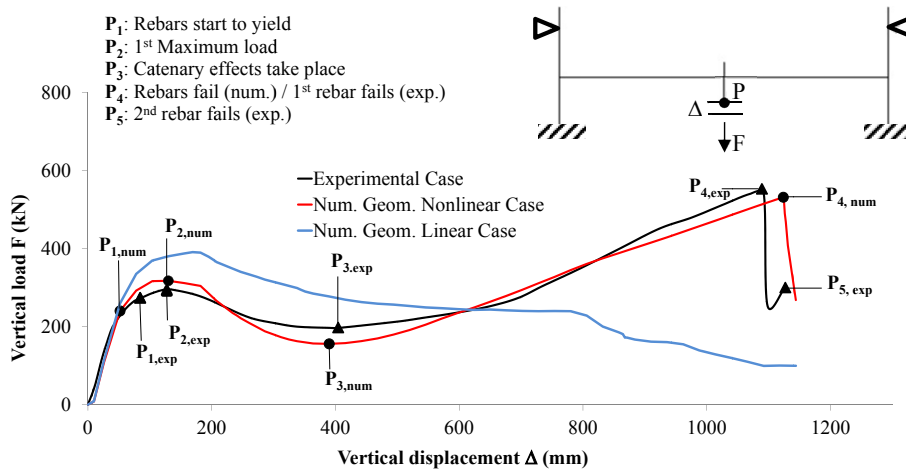
Fig. 4.7. IMF-reference case: load-displacement curve
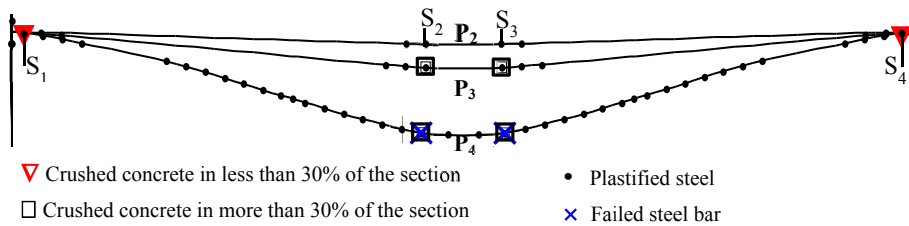
Fig. 4.8. IMF-reference case: structural state at the points defined in Fig. 4.7

Two minor differences are observed, which are perfectly explained by the assumptions used in modelling. The numerical analysis indicates the occurrence of two points of reinforcement bar failure (Fig. 4.8) while during the experiment only the failure on the left side was observed (LEW *et al.* [32]). This is, of course, associated to the full symmetry of the numerical model both from the geometrical and material points of view, which is impossible to guarantee in an experimental test (for more details, see Section 4.4).

The second difference is related to the fact that the experiment shows the subsequent failure of neighboring reinforcement bars, positioned at the same depth of

the section (P_4 and P_5, Fig. 4.7). The numerical model does not allow identifying individual failure of reinforcement bars located in the same sectional layer. Therefore, point P_4 relates to the simultaneous failure of both bottom reinforcement bars in the numerical results (Fig. 4.8).

For the parametric studies, minimum and maximum values of concrete f_c' are taken as 30 MPa and 46 MPa, respectively. The descending branch of the load-displacement curve is affected by the variation of the concrete maximum compressive strength (Fig. 4.9), which confirms the assumption that the decrease of the load is related to the crushing of concrete (LEW *et al.* [32]).

The adoption of $f_c' = 46$ MPa causes an earlier failure of the bottom reinforcement bars at structural sections 2 and 3, as it was observed for the reference case (Figs. 4.7 and 4.8). The potencial causes for this earlier failure are discussed in Section 4.4. Assuming $f_c' = 30$ MPa, nonetheless, leads to the rupture of reinforcement bars in sections near the external columns (Fig. 4.10). This rupture occurs at approximately the same displacement value observed for the reference case, but represents a different failure mechanism. Additional computations assuming the variation of concrete ultimate strain lead to analogous results, resulting in similar load-displacement curves and failure mechanisms (*i.e.*, $\uparrow f_c' \sim \uparrow \varepsilon_{ult,conc}$ and $\downarrow f_c' \sim \downarrow \varepsilon_{ult,conc}$).
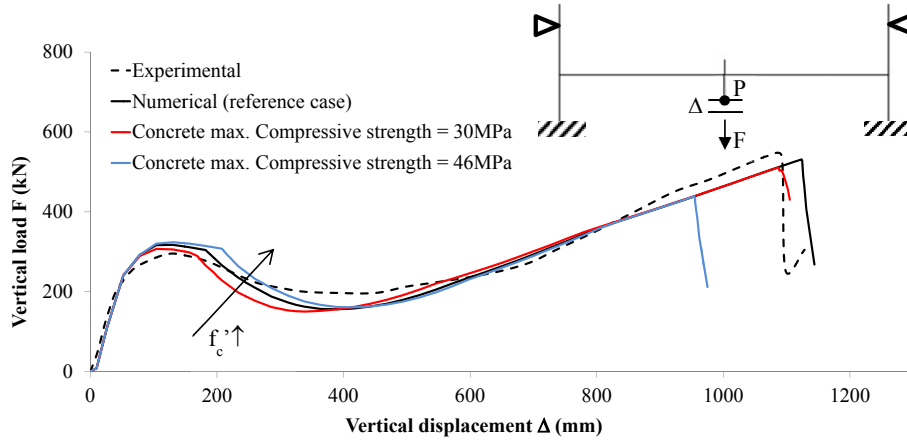

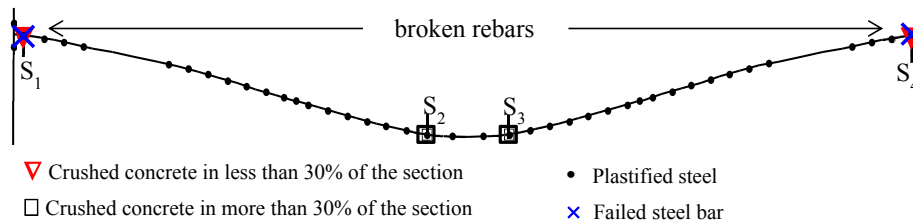**Fig. 4.9.** IMF-variation of f_c': load-displacement curve

Fig. 4.10. IMF-$f_c' = 30$ MPa: deformed shape at the end of the analysis

Now, mininum (516 MPa) and maximum (774 MPa) values of $\sigma_{ult,steel}$ are as-

sumed. According to Eq. 3.35, keeping $\varepsilon_{ult,steel}$ at the reference value and varying $\sigma_{ult,steel}$ can be looked upon as the *variation of the hardening parameter η*. In this case, if $\varepsilon_{ult,steel} = 19.5\%$, the values of η are 0.52 and 3.37, respectively. This variation, as shown in the following, affects the branch of the load-displacement curves (Fig. 4.11) after the first peak load, as well as the displacement level at which the failure of the reinforcement bar occurs.

A lower steel ultimate stress (516 MPa) leads to the failure of the bottom reinforcement bars in structural sections 2 and 3, as observed for the reference case (Fig. 4.8). However, this failure occurs at a lower displacement level. Assuming a higher value for $\sigma_{ult,steel}$ (774 MPa) shifts up the load-displacement curve and prevents the structural failure (Fig. 4.11), *i.e.*, the rupture of steel reinforcement bars does not occur. When additional computations were performed, but assuming variation of the steel ultimate strain instead, a similar behavior is observed for the evolution of the failure mechanism (*i.e.*, $\uparrow \sigma_{ult,steel} \sim \uparrow \varepsilon_{ult,steel}$ and $\downarrow \sigma_{ult,steel} \sim \downarrow \varepsilon_{ult,steel}$). However, increasing or decreasing the value of $\varepsilon_{ult,steel}$ does not have any influence on shifting the load-displacement curve.
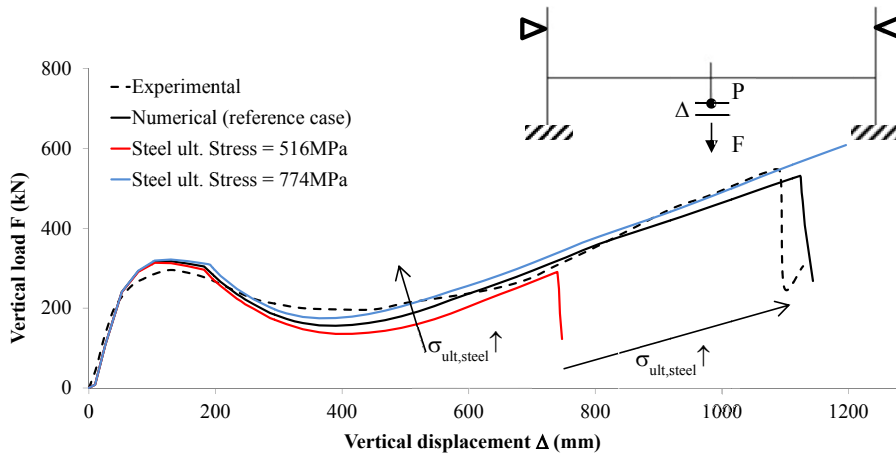
Fig. 4.11. IMF-variation of $\sigma_{ult,steel}$: load-displacement curve

4.3.2 Three-story scale model (TSM)

In this work, the measuring of the vertical displacement of Point P (Fig. 4.4) starts as soon as the gravity load $F = 109.0$ kN is applied. In the results reported in the work of YI *et al.* [33], the mechanical jacks at Point P were released by $N = 7.5$ kN, after what the displacement measurements started.

Using the set of parameters defined in Section 4.2.2, the simulation results in a curve that agrees well with the experimental results (Fig. 4.12). Also, the failure of the reinforcement bars (Fig. 4.13) is consistent with the one observed by YI *et al.* [33]. In the following description of the reference case, the bold numbers correspond to the values measured during the experiment of YI *et al.* [33].

46
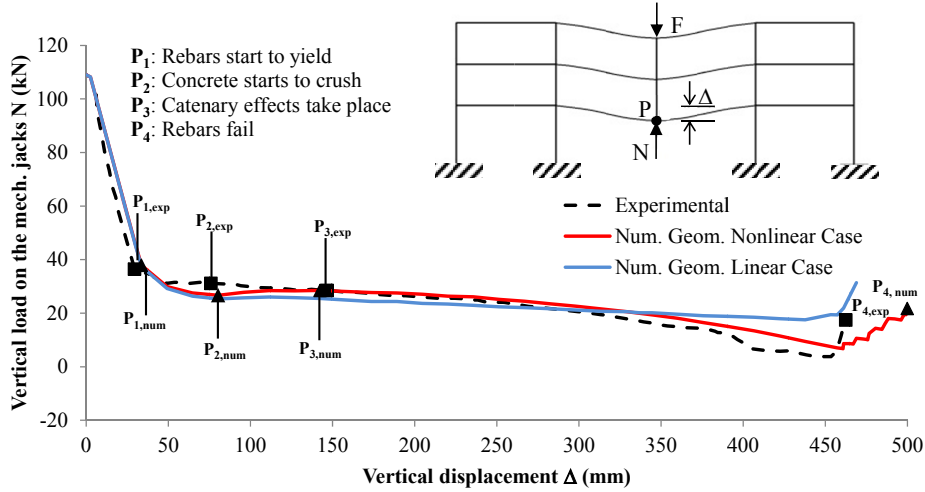
Fig. 4.12. TSM-reference case: load-displacement curve

▽ Crushed concrete in less than 30% of the section   • Plastified steel

☐ Crushed concrete in more than 30% of the section   ✕ Failed steel bar
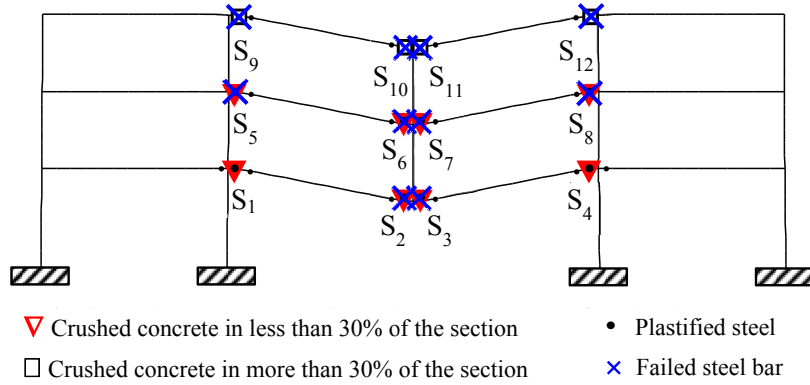
Fig. 4.13. TSM-reference case: structural state at the end of the geom. nonlinear analysis

The Point P_1 in the load-displacement curve (Fig. 4.12) refers to the moment when the first steel reinforcement bars start yielding. This occurred at the same time, at structural sections $1-8$ (Fig. 4.13), at a displacement of $33.7\,\mathrm{mm}/37.9\,\mathrm{kN}$. Yielding of the reinforcement bars is experimentally reported at approximately **29.5 mm/36.4 kN** and is associated to the formation of plastic hinges (YI *et al.* [33]). Concrete starts crushing in compression when the vertical displacement exceeds $80.3\,\mathrm{mm}/26.7\,\mathrm{kN}$ (P_2). In the experiment, severe concrete crushing was reported at **76.0 mm/31.1 kN**. Numerical results show a intense decrease of the reaction force N after the displacements reaches $142.5\,\mathrm{mm}/28.5\,\mathrm{kN}$, indicating the development of catenary actions (P_3). YI *et al.* [33] reported the start of catenary actions at a displacement of approximately **146.7 mm/28.4 kN**.

Experimentally, the rupture of the reinforcement bars at structural section 3 occurred when the displacement was of **462.0 mm/17.4 kN**. This failure caused a sudden increase of the load on the mechanical jacks (P_4). Numerical results show a compound failure of reinforcement bars in several points of the structure (structural

sections 2, 3 and 5 − 12), starting at a displacement of 465.0 mm/8.7 kN (Figs. 4.12 and Fig. 4.13). This compound failure of reinforcement bars is related to the inherent symmetry of loading and geometry in the numerical model. Finally, the failures in structural sections 2 and 3 occurred at 500 mm/21.7 kN, at which point the simulation was interrupted.

Both experimental and geometrically nonlinear cases show a load decreasing trend. On the other hand, an additional geometrically linear analysis results in a load *plateau* between 50 and 450 mm, approximatelly (Fig. 4.12). The failure mechanism of the geometrically linear case is also different from the one obtained with the geometrically nonlinear analysis, resulting in higher levels of concrete crushing and, more importantly, different points of reinforcement bar failure (Figs. 4.13 and 4.14). These outcomes reaffirm the overall enhancement of the structure by catenary effects and motivate the use of large displacement analysis for capturing the correct structural response, including the failure mechanism.
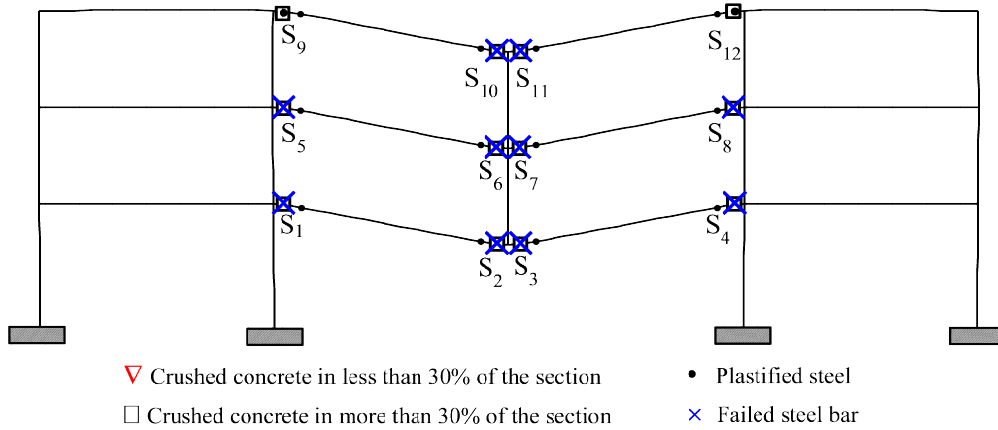
Fig. 4.14. TSM-reference case: structural state at the end of the geom. linear analysis

The values adopted for steel ultimate strength during the TSM parametric studies are equal to 512 MPa and 768 MPa. The corresponding hardening parameters are (η) equal to 0.4 and 4.5. This variation only affects the load-displacement curve after the point related to the yielding of the reinforcement bars and is illustrated in Fig. 4.15. Basically, lower steel strength values move the numerical curve upward, while higher values do the opposite. However, the general shape of the curve is not affected and the decrease of the vertical load on the mechanical jacks is still reproduced after the catenary effects start. The minimum value assumed for the steel ultimate strength results in the failure of structural sections 2 and 3 (see Fig. 4.13 for section identification), after what the analysis was interrupted. When the highest value is considered, more yielding points are displayed, as well as points of concrete crushing. Even though the resulting load-displacement curve is very similar to the experimental case (Fig. 4.15), the failure of the reinforcement bars is not

observed.
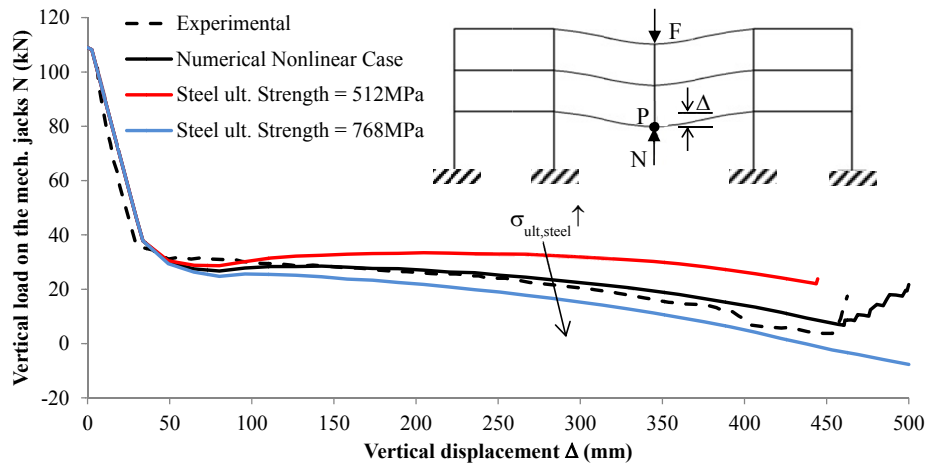
Fig. 4.15. TSM-variation of $\sigma_{ult,steel}$: load-displacement curve

For the case of steel ultimate strain variation, minimum and maximum values are 10.0% and 15.0%. These values, applied to Eq. 3.35 along with a fixed $\sigma_{ult,steel} = 640\,\mathrm{MPa}$, provide hardening parameters (η) equal to 3.1 and 2.0, respectively. The load-displacement curve is not significantly affected, except for the point that represents reinforcement bar failure (Fig. 4.16). The assumption of $\varepsilon_{ult,steel} = 10.0\%$ leads to an earlier compound failure with a similar mechanism as the one observed for the reference case (Fig. 4.13). When the higher value is considered, the reinforcement bars do not break and the load increase at the end of the curve is not reproduced (Fig. 4.16). These results, as for the IMF-case, confirm that the use of reinforcement bars with higher strength and ductility would prevent the progressive collapse of this structure in the considered displacement/load levels.
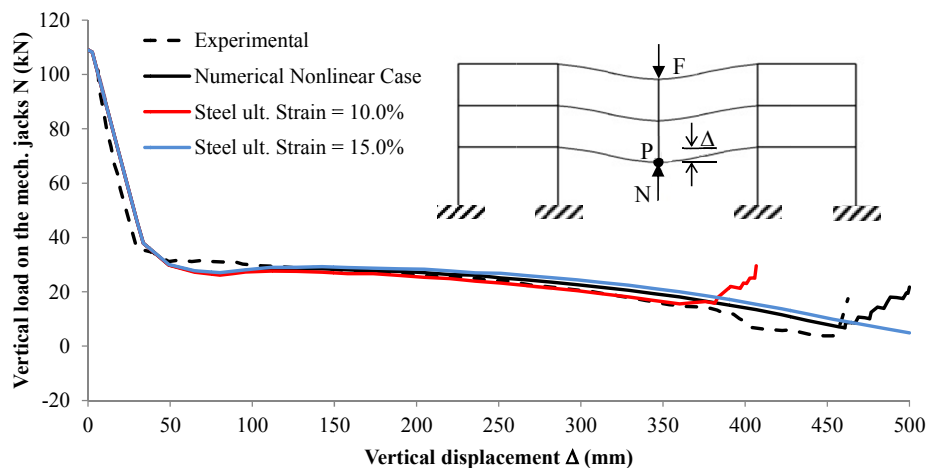
Fig. 4.16. TSM-variation of $\varepsilon_{ult,steel}$: load-displacement curve

Additional studies concerning the concrete maximum compressive stress (24 and 36 MPa) and ultimate strain (0.32 and 0.48%) were performed. No significant change

49

of the load-displacement curve is reported and the curves obtained are very similar to the one on Fig. 4.12. The reference compound failure mechanism remains the same (Fig. 4.13) for all the cases, except for the one in which $f'_c = 24\,\text{MPa}$. For that case, the structural state at the end of the analysis is shown on Fig. 4.17.
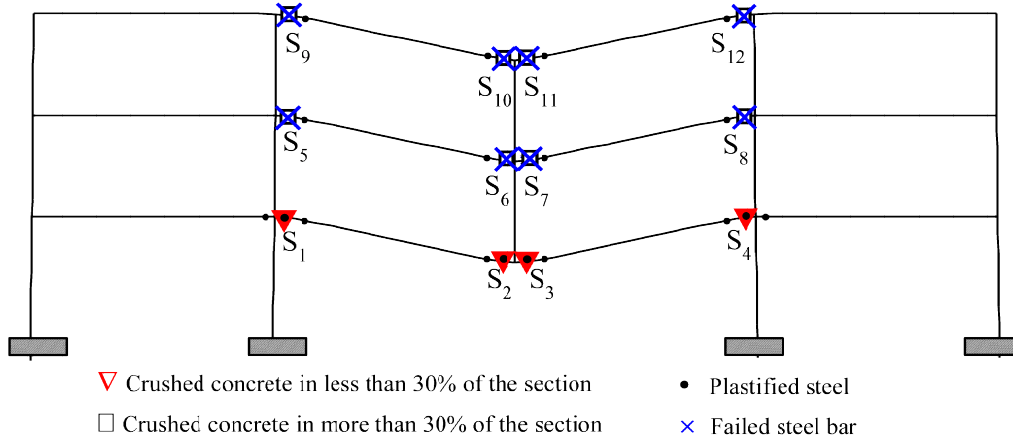
Fig. 4.17. TSM-$\sigma_{ult,steel} = 631\,\text{MPa}$: structural state at the end of the analysis

4.4   Discussion of the Results

The association of a Bernoulli beam element and a multilayer corotational formulation was effective in reproducing the experimentally observed structural behavior of two models. Very good agreement was obtained. Steel yielding and concrete crushing, among other features, were displayed at the experimentally observed load and displacement levels. Results in terms of load-displacement curves and failure mechanisms were appropriately reproduced and the goal of establishing a direct correlation between numerical and experimental simulations is clearly achieved. This was only possible with the correct identification of the geometric properties of the structures and the right description of the material behavior. Still, it was necessary to resort to supplementary references for building the reference cases, enforcing the necessity of providing as much relevant experimental data as possible when describing simulations and correctly linking sources, in order to permit the reproduction of the tests.

Geometric nonlinear effects (catenary effects) were quantified and shown to considerably enhance the overall strength of both structures. This indicates that the inclusion of these effects is crucial for describing the correct structural response, since this enhancement could not be captured by a formulation based on a geometrically linear description. The numerical analysis of the TSM showed that only the floors located above the removed column were affected. This localized damage is considered to be a positive aspect since, in case of reparations, interventions would

only be necessary on the affected floors. This also has implications for acceptability criteria with respect to PC as defined in some codes, using a concept of allowable collapse region (DoD [71]). Of course, TSM represents a reduced scale model of the first three floors of the building and the replication of this effect should be verified for the complete real size model in a dynamic analysis.

In the experimental works of LEW *et al.* [32] and YI *et al.* [33] the removal of the column was simulated in a quasi-static manner by applying a monotonically increasing displacement at the connection with the failed member. An approach like that does not included the dynamic effects (vibrations, strain rate effects, viscoplasticity, etc.) that are part of the real PC phenomenon. The investigation of considering all of these effects in a large displacement scenario is presented in Chapter 5.

The Bernoulli beam formulation used in this chapter does not include shear effects and the physical presence of stirrups is not incorporated in the finite element formulation. This means that their positive influence in preventing concrete cracking, if any, is neglected. However, a 20% increase was assumed for the concrete maximum compressive strength in order to artificially account for the concrete confinement. As assumed by IRIBARREN *et al.* [36], the concrete constitutive model ignores the structural strength associated to tensile loading.

The efficiency of computational simulations in predicting the different structural behaviors associated to the use of different materials was reaffirmed with the results of the parametric studies. After twenty analyses were performed, two different failure mechanisms were identified for IMF and three for TSM, excluding the ones on which there was no reinforcement bar failure. In an experimental basis, the cost of building and testing the same number of structures would be prohibitive. During these studies, the values of steel ultimate strain were as high as 23% and variation of this parameter caused the change of the failure mechanism of both structures.

The IMF experimental failure was reported to happen on structural section 2 (LEW *et al.* [32]), while the numerical simulation pointed out failure of structural sections 2 and 3 (Fig. 4.8). More interestingly, for the TSM, YI *et al.* [33] reported the single failure of structural section 3, contrasting to the multiple section failure observed in the numerical analysis (Fig. 4.14). The explanation for these differences is based on the fact that the geometry and the boundary conditions of both structures naturally lead to perfectly symmetric numerical models, including the loading pattern and the material properties. Such condition of perfect material symmetry is impossible to reproduce in experimental tests. In order to verify the validity of this argument, an additional simulation for TSM was performed, turning structural section 3 into a "weak point". The steel ultimate strength on that section was reduced by 5% of the reference case, simulating asymmetry and material heterogeneity. The exact failure mechanism described by YI *et al.* [33] was then

reproduced, at a displacement of 459.2 mm (**459** mm). This shows that numerical results are indeed consistent with the experimental structural behavior if performed with similar initial conditions.

By nature, the multilayer discretization adopted here is not capable of identifying the single failure of neighboring reinforcement bars in a discrete layer at the same cross sectional height. Instead, the simultaneous failure of all reinforcement bars will always be identified as the failure of the complete layer(s). The association of a fiber discretization in a three-dimensional analysis and a statistically based distribution of "weak points" in the reinforcement bars would provide an even more realistic numerical model and overcome this limitation.

The parametric studies also demonstrated that the IMF structure was strongly sensitive to the variation of concrete maximum compressive strength and ultimate strain. This variation can be result of, for instance, different concrete confinement conditions (MANDER *et al.* [81, 89]). The drop of the load-displacement curve in Fig. 4.9 shows that higher values of those parameters induce an earlier failure of the structure. The experimental results in LEW *et al.* [32] indicate that these effects start after the load is stabilized at **196** kN, at a displacement of **406** mm (Fig. 4.7, P_3). In fact, this point of the curve represents the moment when the catenary effects make themselves clearly present in the structural behavior. Another definition on the onset of these effects can be given, based on layer stresses from the computation, as the appearance of tension in at least one of the reinforced layers that were previously under compression. When adopting this definition, it is possible to verify that the first sign of the catenary effects appears even before concrete starts to crush. The layer discretization used in this work allows investigating this process and indicates that concrete crushing interacts with the full development of the catenary effects and, later on, with the structural failure.

The following interpretation is proposed, based on IMF numerical results obtained for structural section 1 (Fig. 4.7):

i) As the displacement increases, the reinforced layers that were once under compression start to enter the tensile zone (Fig. 4.18);

ii) When concrete starts crushing, the sectional area changes, forcing the reorganization of the sectional stresses. As a result, the tensile stresses in the reinforced layers decrease and some of them return to the compressive state (Fig. 4.19);

iii) If there is no more crushing of concrete layers, tension starts to increase again and new composite layers are submitted to tension.

As a result of this process, the development of catenary effects is not systematically interrupted when concrete exhibits higher f'_c, *i.e*, the increasing of the tensile stresses in the reinforced layers is more continuous. When compared to the lower $f'_c = 30$ MPa case, this uninterrupted increasing of stresses results in higher ten-

sile stresses at a same displacement/load level and leads to ealier reinforcement bar failure (Fig. 4.8). The same analysis explains the earlier failure of a structure with higher concrete ultimate strain in comparison to the reference case. This interaction between concrete crushing and catenary effects leads to a very complex structural behavior which cannot be easily anticipated or explained without the additional insight given by the multilayered discretization.
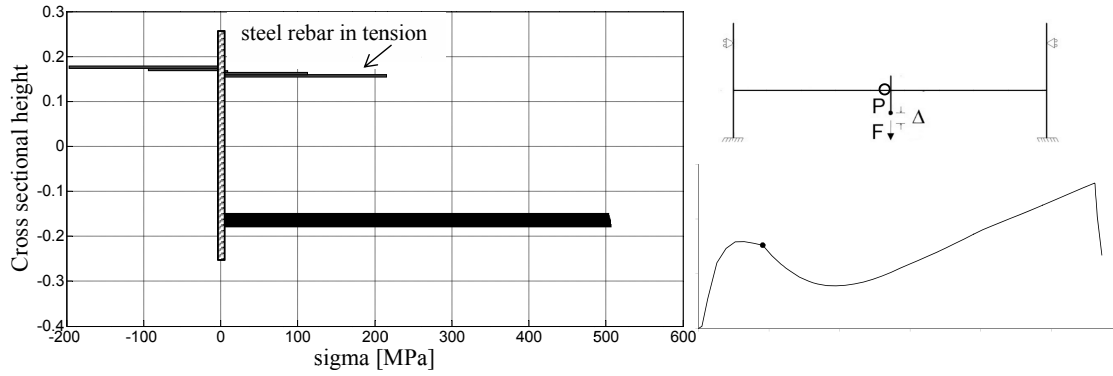

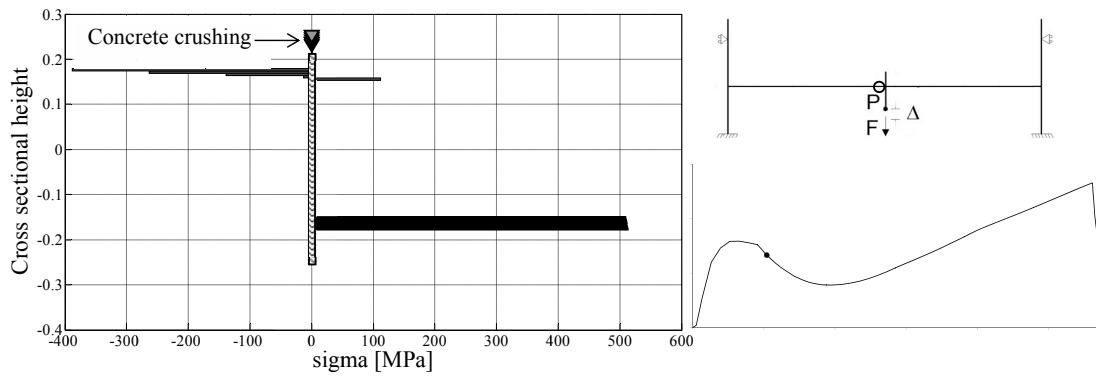**Fig. 4.18.** IMF-reinforcement bar stress distribution, before concrete crushing (structural section 2, Fig. 4.7)

Fig. 4.19. IMF-reinforcement bar stress distribution, after concrete starts crushing (structural section 2, Fig. 4.7)

Chapter 5

Design Code Comparison and Dynamic Progressive Collapse Analysis of a Five-Store Building

The main purpose of this chapter is the computational investigation of the structural response of two planar frame models that represent a five story reinforced concrete (RC) building, designed in accordance with EUROCODE [37] and the Brazilian building code NBR 6118 [40][1]. Even though sharing the same architectural geometry, since these codes prescribe different requirements, the obtained models are different in terms of loads, element cross sections, reinforcement scheme, reinforcement ratio, and consequently, in terms of structural robustness. More detailed information on these models and their design process are presented and discussed hereafter.

The previous section demonstrated the capacity of the multilayered approach to capture complex structural response via experimental-numerical agreement. Here, ingredients related to features of Progressive Collapse (PC), *i.e.*, dynamics and strain rate effects are included in the formulation for the study of realistic PC scenarios.

5.1   Structural Design

The plane frames consist of an 18 m high office building with five levels. The ground floor height is 6 m and the height of the other floors is 3 m. The frame is 48 m long, equally divided in 6 m bays as shown in Fig. 5.1. Since the presented work aims at investigating the influence of catenary effects due to the large changes in the geometry, the removal of an interior column was considered. A similar procedure was adopted by LEW *et al.* [32] and YI *et al.* [33].

---

[1]Partially developed during the participation of the reseacher on the Programa de Doutoramento Sanduíche no Exterior, at the Université Libre de Bruxelles, in Brussels/Belgium.
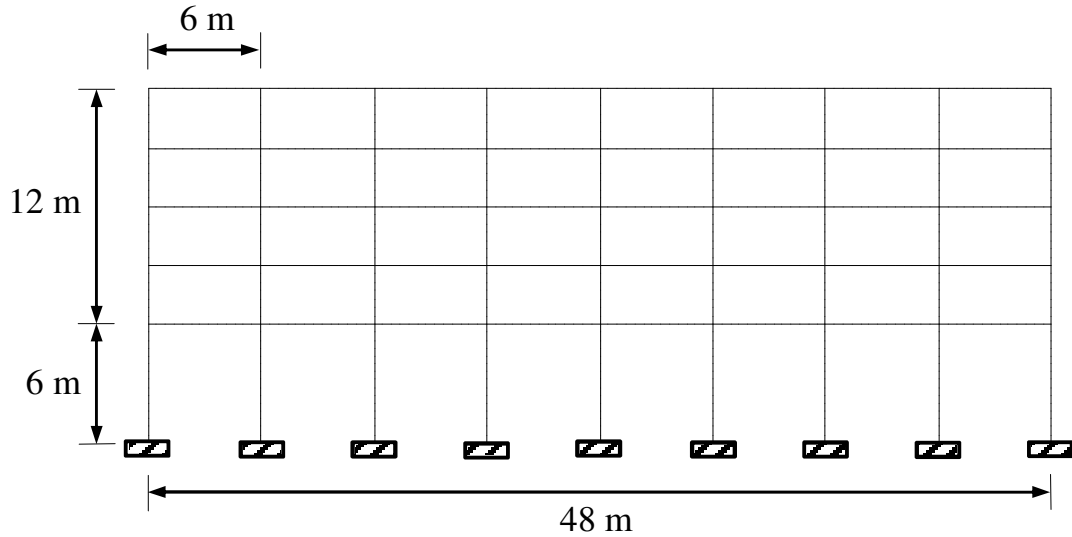
Fig. 5.1. Architectural design

The Eurocode-based design was carried out using the commercial software Diamonds (BUILDSOFT NV [97]) and presented in IRIBARREN [63] and IRIBARREN *et al.* [36], from where the parameters used in this work were directly taken. The material parameters and geometry of the structural elements therefore consider European practical values. On the other hand, the Brazilian design was specifically performed for this work on Cypecad (CYPE [98]), assuming the minimum specifications of NBR 6118 [40].

Thirty centimeters thick concrete slabs were used for the Eurocode-based frame, including a concrete cover layer of 10 cm. As discussed by LEE and SCANLON [99], EUROCODE [37] does not define minimum thickness for concrete slabs. Instead, the thickness is obtained as a function of the final reinforcement ratio. The European design assumes minimum reinforcement ratio (IRIBARREN *et al.* [36], IRIBARREN [63]), therefore it is correct to assume that the thickness of 20 cm used in that work is also minimum. Slabs of 13 cm are used for the Brazilian design (without any cover layer). The lack of a cover layer in the Brazilian building is justified by the herein assumed methodology of obtaining a design based on minimum requirements. These slabs do not provide any resistance; however, they were adequately dimensioned and verified against maximum allowable displacements.

Live and dead loads are summarized in Table 5.1. The total load, shown in the same table, combines the total dead load value with 50% of the live loads, as recommended by DoD [71]. The multiplication of the reinforced concrete weight density (24 kN/m^3) by the volume of the structural element and subsequent division by its length gives the self-weight load, translated into loads per unit length (for self-weight of the slabs, the length is taken as the beam length):

- for the Eurocode-based frame:

$q_{dead}=$ (0.30 m $\times$ 6 m $\times$ 6 m $\times$ 24 kN/m^3) /6 m = 43.2 kN/m

- for the NBR-based frame:

$q_{dead}=$ (0.13 m $\times$ 6 m $\times$ 6 m $\times$ 24 kN/m^3) /6 m = 18.7 kN/m

Table 5.1
Recommended beam loads

Loads (kN/m)	Dead	Live	Total
Eurocode [37] based design			
Floor Beams	43.2	18.0	52.2
Roof Beams	43.2	6.0	46.2
NBR 6118 [40] based design			
Floor Beams	18.7	12.0	24.7
Roof Beams	18.7	6.0	21.7

The following assumptions were made during the design process:

- all floor beams are the same, since the same loads were considered at all floors;

- all columns are considered the same, *i.e.*, although upper floor columns bear smaller loads, they have the same section and reinforcement scheme as ground columns;

- the height and the width of a structural element are constant along the length;

- assuming Aggressiveness Class II, the NBR-based design has a concrete reinforcement bar cover of 2.5 cm; a 5 cm concrete reinforcement bar cover is taken for the European design, as in IRIBARREN [63] and IRIBARREN *et al.* [36];

- the bottom reinforcement is assumed continuous in both designs;

- the continuity of 2/3 of the top beam reinforcement (Fig. 5.2) is considered in both designs;

- bond and anchorage were considered during the design process but are not included in the progressive collapse analysis;

- perfect bonding between concrete and steel is assumed;

- stirrups are considered during design, but not represented in the PC analysis, *i.e.*, the increase in the concrete strength and ultimate strain resulting from the confinement are not taken into account.

Although the design of the Eurocode-based building is the same as the one presented by IRIBARREN [63] and IRIBARREN *et al.* [36], the present analysis applies a further developed numerical formulation that includes nonlinear geometrical effects (catenary effects). Another difference resides in the fact that concrete strength under tension is not taken into account here, based on usual reinforced concrete practice. Besides, the influence of strain rate effects was not taken into account in IRIBARREN [63] for the case middle column removal.
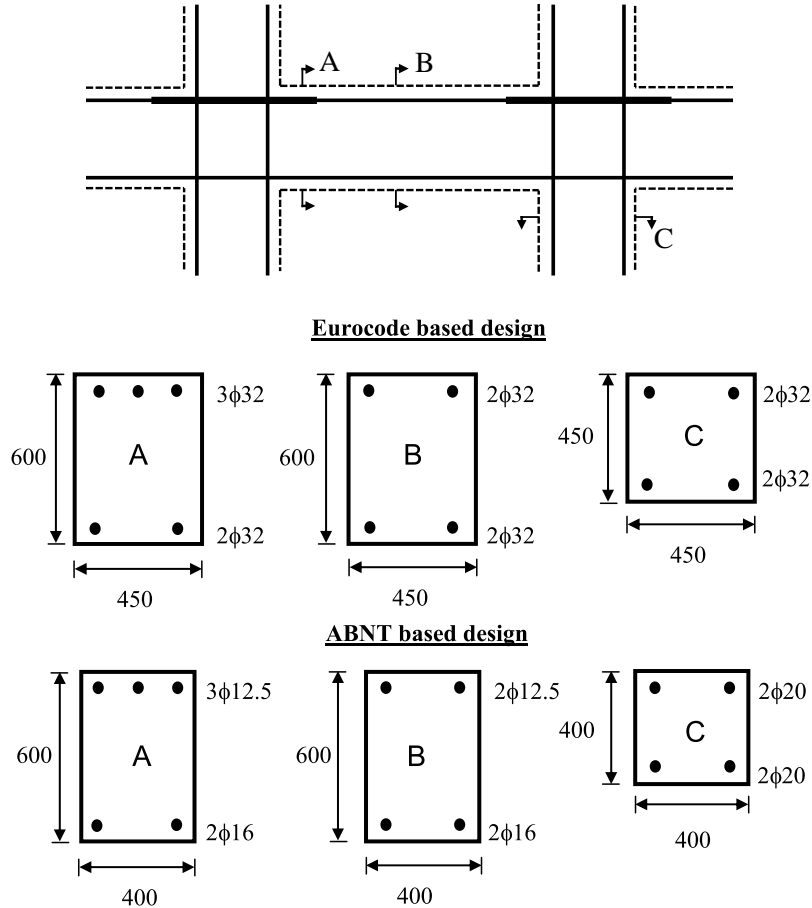
Fig. 5.2. Reinforcement schemes
(all values are given in milimiters)

5.2 Material Constitutive Behavior

Based on EUROCODE [37], class C30 concrete and S500 steel were used for the European structural design. As mentioned before, the design process of the Brazilian structure was aimed at producing a frame based on the minimum parameters of NBR 6118 [40], including the material properties as concrete strength and steel strength. C20 concrete is the lowest concrete class allowed by NBR 6118 [40], except for reinforced concrete foundations, for which it is acceptable to use C15 concrete. For

that reason C20 concrete was adopted for the Brazilian structure in association with CA50 steel bars.

The constitutive model for these materials is described through a bilinear approximation of the stress-strain behavior, based on recommendations established by EUROCODE [37] and *fib* [38, 39] (Fig. 5.3). The following assumptions are used to define this simplified model:

- although in some scenarios tensile stresses may play a non-negligible role in structural strength, any structural strength associated with tensile loading is not taken into account, *i.e.*, concrete under tension is considered to be fully cracked and the corresponding tensile stresses are neglected;

- strains and stresses are linearly proportional on the ascending part of the curve, as recommended by EUROCODE [37], instead of the nonlinear curve proposed by *fib* [38, 39]. Young's moduli were set as 32 GPa for C30 and 25 GPa for C20 concrete, respectively;

- for quasi-static loading conditions, the plastic regime is represented by a *plateau* at a stress of 37.9 MPa for C30 concrete and 20 MPa for C20 concrete;

- the ultimate strain under compression in both types of concrete is defined as 0.35%, after which any increase in the strain level will immediately decrease the stress to zero and keep it at this level in the subsequent loading steps.
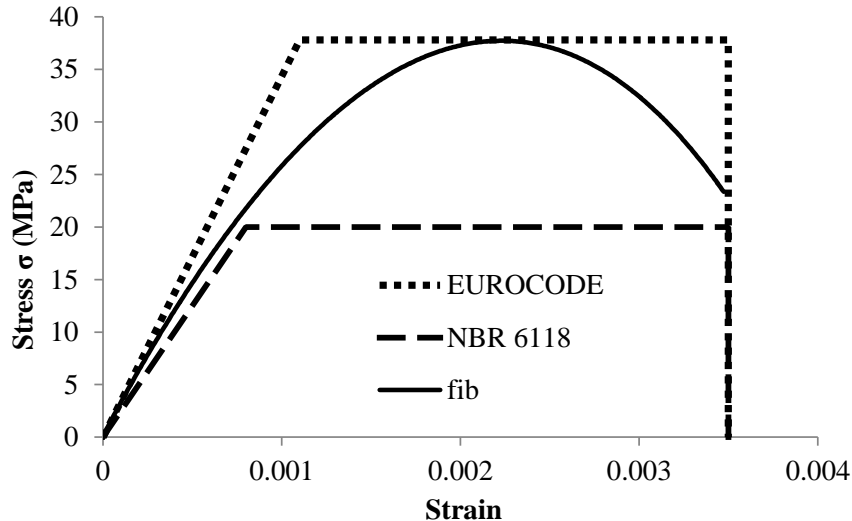
Fig. 5.3. Constitutive model - concrete in compression for quasi-static loading

Based on EUROCODE [37] and NBR 6118 [40], the bilinear curve on Fig. 5.4 was defined to represent the relationship between stress and strain for steel under quasi-static loading conditions. The following additional information can also be related to the constitutive behavior of S500 steel and CA50 steel:

58

- the steel behavior in tension is analogous to the one in compression;

- the buckling of compressed steel bars is not taken into account;

- the elastic modulus, yield stress and ultimate strain are equal to 200 GPa, 500 MPa and 4%, respectively;

- the Brazilian code NBR 7480 [100] states that the ultimate strain for CA50 steel is equal to 5%. However, to remain true to the proposed comparison with IRIBARREN [63] stresses in the steel vanish as the strain reaches values larger than 4%, representing steel fracture;

- the ratio between ultimate stress and yield stress is equal to 1.06 (IRIBARREN *et al.* [36], IRIBARREN [63]).

Strain rate effects on the behavior of steel and concrete were included as in IRIBARREN [63] and IRIBARREN *et al.* [36] (Section 3.2.6).
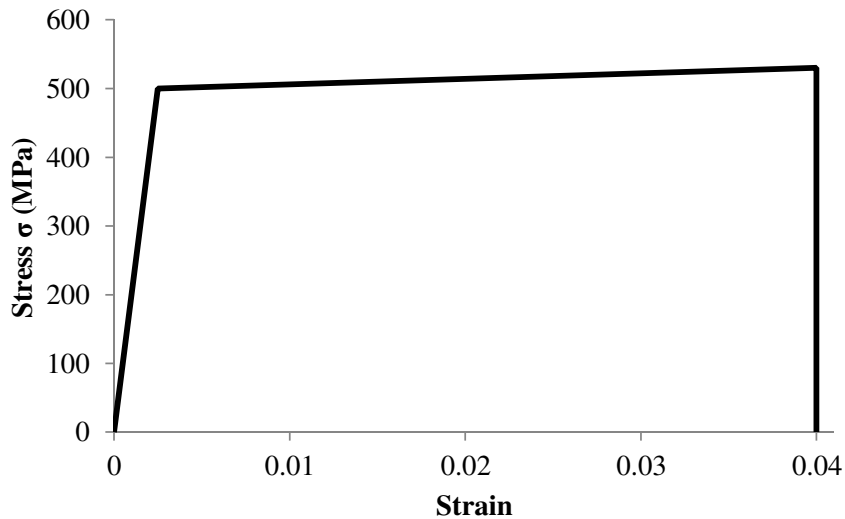
Fig. 5.4. Constitutive model - steel for quasi-static loading

5.3 Computational Results

Each plane frame has the same 2D discretization, constituted from approximately 900 beam elements. Forty layers are used for the discretization of the columns cross sections and sixty layers for the beams, numbers that were defined after a study on the convergence of the numerical analysis. The structure self-weight and service loads are applied in a large period of time, defined as 1000 s, in order to prevent the influence of dynamic effects in the initial loading phase, which is ideally quasi-static. The column removal is modeled as the decrease of the reaction forces, equivalent to the presence of the 5th ground column, applied at point E (Figs. 5.5 and 5.6). This

is done in a short period of time (0.01 s), subsequently to the initial loading process. The response of the structure is analyzed for a period of two seconds after column removal, as in IRIBARREN [63] and IRIBARREN *et al.* [36]. The removal time corresponds to 0.5% of the response time, which classifies the loading as *impulsive* (SMITH and HETHERINGTON [101]).
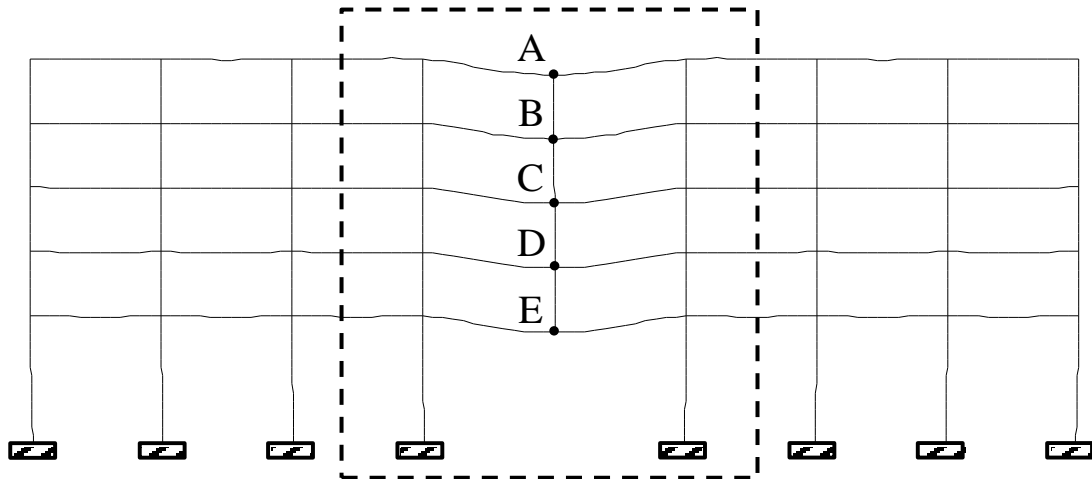
Fig. 5.5. EUCO's deformed configuration
(displacements multiplied by 10, dashed lines relate to Fig. 5.8)
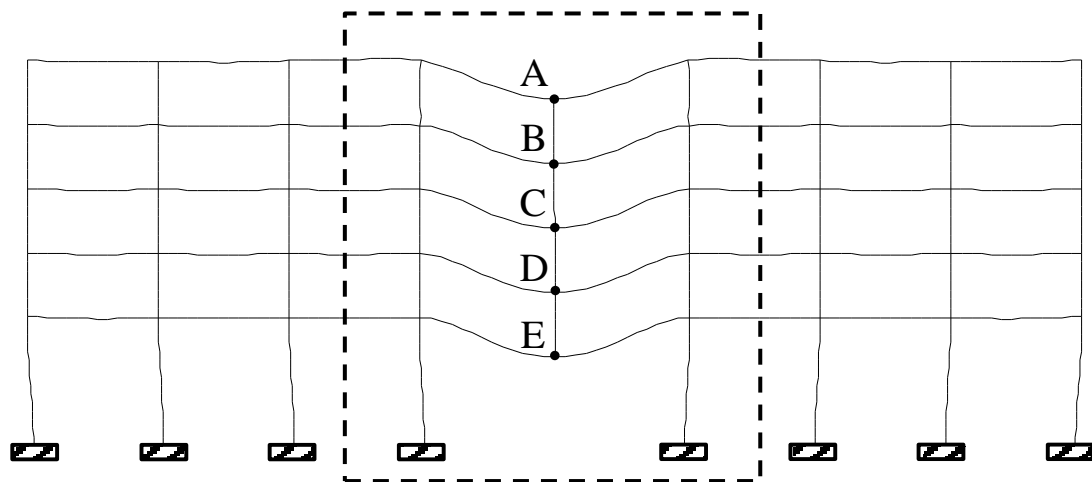
Fig. 5.6. BRCO's deformed configuration
(displacements multiplied by 10, dashed lines relate to Fig. 5.9)

The removal of a column results in the inversion of the bending moments applied on the beams which must resist these changes. Results show that the reinforcements did not fail. Consequently the structures did not collapse with the middle column removal, *i.e. both structures were able to overcome the loss of the column and did not initiate the progressive collapse mechanism, according to the simulation.* The deformed configuration of the EUCO (Eurocode-based frame) and BRCO (NBR-based frame) is shown in Figs. 5.5 and 5.6, respectively, which make clearly noticeable that

the displacements in BRCO are larger. In fact, BRCO's vertical displacements on the reference points A-E are approximately 2 times larger than the ones of EUCO (Table 5.2). The displacement values shown on Table 5.2 also imply that the columns located between points A and E (Figs. 5.5 and 5.6) undergo rigid body motion.

Table 5.2
Vertical displacements (cm) at reference points
(at times denoted by point P3 on Fig. 5.7)

Reference Point	EUCO (V_1)	BRCO (V_2)	$\frac{V_2}{V_1}$
A	−9.61	−19.2	2.00
B	−9.65	−19.3	2.00
C	−9.71	−19.4	2.00
D	−9.76	−19.5	2.00
E	−9.78	−19.6	2.00

Within the time interval defined by points P1 and P2 in Fig. 5.7, the mean value of the displacement of point E (Figs. 5.5 and 5.6) is of approximately 8 cm and 18 cm for EUCO and BRCO analysis, respectively. Table 5.2 displays the vertical displacements of the reference point E for both structures. As the structures have different frequency of the displacement oscillation, the values shown on Table 5.2 were taken as the largest immediate displacements before the analysis completion, identified on Fig. 5.7 by point P3.
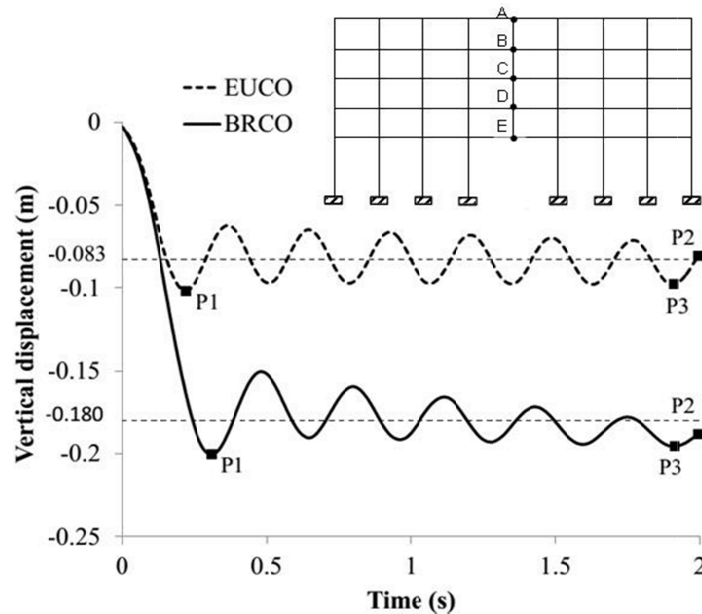
Fig. 5.7. Vertical displacement of point E, as a function of time.

The frequency of the displacement oscillation is slightly higher for EUCO frame. In terms of natural frequencies, this result indicates that the increase factor of

61

EUCO's stiffness was higher than the increase factor of its mass. The relation described is given by:

$$\omega = \sqrt{k/m} \tag{5.1}$$

where ω, k and m represent, respectively, the natural frequency, the structural stiffness and the mass of the body.

Besides, BRCO's structural elements have smaller sections and less reinforcement leading to a lower stiffness and the material behavior adopted for concrete in the two simulations is different as well (Fig. 5.3). These are the explanations for the larger displacements of the Brazilian frame.

The state of individual structural members at any time in the simulation is available from the numerical simulations. In Figs. 5.8 and 5.9, the symbol (.) was used to represent sections in which steel has reached yielding and ($\bigtriangledown$) represents those in which concrete was crushed in less than 30% of the layers. It can be seen that, for both frames, the effects of the middle column removal can barely be identified on other beams and columns than the ones above the point E. However, Figs. 5.8 and 5.9 show that BRCO presents a larger number of plastified sections (158 sections from BRCO against 94 sections from EUCO). Differently from EUCO, BRCO also displays sections on which concrete was crushed.
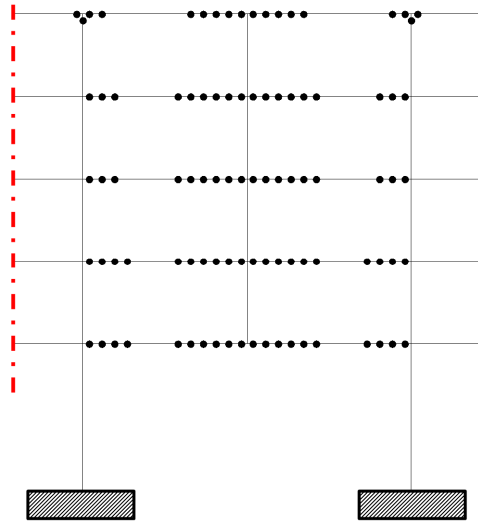
Fig. 5.8. EUCO's plasticity distribution on the undeformed configuration, at the end of the analysis (2 s after middle column removal; for the sake of good visibility, only the afected areas we represented)

According to the *Allowable Collapse Region* criterion (DoD [71], EUROCODE [78]), only the bays immediately adjacent to the removed element must be affected. This indicates that only bays 4 and 5 could be affected in terms of collapse. Figures 5.8 and 5.9 show that there was no collapse and that plastification of the steel
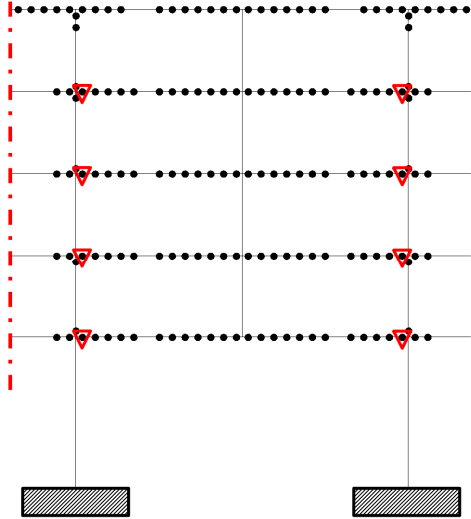
Fig. 5.9. BRCO's plasticity distribution on the undeformed configuration, at the end of the analysis (2 s after middle column removal; for the sake of good visibility, only the afected areas we represented)

reinforcement bars only occurs in bays 4 and 5. Therefore, the *Allowable Collapse Region* criterion was fulfilled.

5.4   Discussion of the Results

The preliminary assumption of having structural models designed in accordance to EUROCODE [37] and NBR 6118 [40] also resulted in using different constitutive behaviors for concrete. As seen in Fig. 5.3, BRCO considers lower yield strength of concrete. Using a higher class concrete in the BRCO minimum requirement design may however not systematically lead to an increase in the overall robustness of the structure. This would also result in different cross sections for the structural elements and different reinforcement schemes during the structural design step. Therefore, a new set of PC simulations should be conducted to assess the influence of such a variation.

Given the multiscale approach of the PC problem discussed here, it was necessary to define an optimum number of layers for discretizing the members cross sections, i.e. not too many layers that would make the analysis unafordable in terms of computational time or too few that would introduce significant errors in the results obtained. For every new design a similar preliminary step is advised to establish the minimum number of layers to be used for the element cross sections.

For this work, the complete multiscale PC analysis of one structure took approximately 8 hours on an Intel i5 3.0 GHz computer, using a single CPU core for the computation. The computational performance could be significantly enhanced using a parallel computation scheme.

63

The oscillation of the point above the removed column is of high importance, since it implies repeated cyclic variations of the structural stress level. This scenario may accelerate the process of concrete crushing and introduce material damage.

Both designs were able to resist PC, and the plastic strain distribution was localized in the two bays above the removed column. This type of localized damage may be seen as a restricted damage extent, thereby decreasing the number of losses, and resulting in easier reparation of the remaining structure. Nevertheless, it is important to stress that the plasticity distribution and structural damage may be strongly dependable on the position of the removed column (IRIBARREN *et al.* [36], IRIBARREN [63]), and a more wide-spread damage may be expected in other scenarios.

Additional analyses using a geometrically linear formulation showed a response similar to the one described earlier. This implies that the positive influence of (geometrically nonlinear) catenary effects in mitigating PC could not be triggered in the considered simulations due to the relatively small displacements in the structure. However, this point could be further investigated in future works in 3D simulations and also in the analyses of different RC frame models.

Chapter 6

Conclusion and Perspectives

This work presented the computational analysis of reinforced concrete (RC) plane frames aimed at investigating the propagation of damaged cased by the loss of a column and at the tendency to the development of the so-called progressive collapse (PC). The problem of PC was approached taking into account material and geometrical nonlinearities in quasi-static and also dynamic scenarios. A multilayered Bernoulli beam element using corotational kinematics was developed for this purpose.

Chapter One introduced the problem of the PC of RC buildings, presenting examples throughout the world. The main originalities and contributions were also presented in Chapter One, as well as the scope of the thesis. An extensive bibliographic research was performed for this work and was summarized in Chapter Two. The chapter stated the importance of the many ingredients included in the proposed numerical approach. Chapter Three described the nonlinear dynamic formulation of the multilayered Bernoulli beam element, including the geometrically nonlinear kinematics, material nonlinearities, strain-rate effects and viscoplastic effects. A quasi-static approach was assumed in Chapter Four for modelling two reinforced concrete structures in order to establish a direct correlation between experimental and numerical analysis. The structures were selected from the literature which provided complete information on the geometry, on the material properties and also experimental data for comparison to the results of the numerical simulation. Chapter Four also includes a summary on the correlation between the experimentally observed material behavior and the constitutive models used in the simulations. Chapter Five aimed at comparing the tendency for progressive collapse of two reinforced concrete buildings designed in accordance with the minimum requirements of two different building codes, from Europe and from Brazil. The objective was to verify if the minimum requirements of those codes were adequate structural safety and robustness in order to prevent the occurrence of progressive collapse. The details and assumptions made during the design process were given, as well as a summary

of the applied numerical formulation and the material constitutive behavior.

6.1   Concluding Remarks

The formulation proposed in this work was successful in coupling the different proposed ingredients (geometric and material nonlinearities, in a dynamic scenario, including strain rate effects and viscoplasticity). Therefore, it is fair to say that the association of the multilayered discretization of the cross section and the corotational kinematics of a Bernoulli-based beam element was also successful. This formulation was applied to the progressive collapse analysis of reinforced concrete buildings and produced the following results:

- to what concerns the correlation between experimental and numerical approaches, load-displacement curves are in very good agreement with the experimentally measured data. This indicates that the exercise of producing a numerical model having the experimental data as base was correctly conducted;

- the experimentally observed structural behavior, as the yielding and failure of steel reinforcement bars, concrete crushing and the development of catenary effects, were correctly reproduced;

- the enhancement of the structural strength resulting from catenary effects was confirmed for both IMF (Intermediate Moment Frame) and TSM (three-story scale model), highlighting the importance of performing geometrically nonlinear (large displacements) analysis;

- the numerical parametric studies revealed that the failure mechanism of both IMF and TSM was very sensitive to the variation of some key material parameters, even though the general shape of the load-displacement curves were not severely affected;

- the artificially introduction of the confinement effect of stirrups on concrete, *i.e.* the increase of maximum concrete compressive strength $(f_c^{'})$ in 20%, was significant to the correct description of the models behavior. This statement is confirmed by the parametric studies which showed that, when a lower $(f_c^{'})$ was considered, different load-displacement curve and failure mechanism were observed for the IMF and for the TSM, respectively;

- the differences between experimental and numerical failure of the reinforcement bars in the IMF model were demonstrated and explained to be related to geometrical and material asymmetry;

- with respect to the comparison between building codes, larger displacements associated to lower vibrational frequencies were observed for the NBR based design frame as a result of weaker design constraints and lower stiffness of the structural system, which also resulted in a higher number of plastified steel sections in that structure;

- the presence of stirrups was not (artificially or physically) included in the analysis for building code comparison. However, based on the results of the correlation between numerical an experimental approaches, it is believed that accounting for the concrete confinement provided by the stirrups would be beneficial to the integrity of the structures;

- for both NBR and Eurocode-based designs, the structural damage happened to be localized only on the floors immediately above the removed middle column. However, since there was no signs of additional failure, the *Allowable Collapse Region* criterion (DoD [71], EUROCODE [78]) was fullfilled;

- none of the structures triggered the progressive collapse mechanism after the removal of a middle column, which implies that the minimum requirements of both codes are successful in providing structural robustness for the particular scenarios studied here under the 2D assumption.

6.2   Perspectives for Future Works

Future research includes:

- the update of the proposed multilayered Bernoulli beam formulation to a Timoshenko beam formulation in order tho model shear effect and the confinement effect of stirrups on concrete;

- a correlation between experimental and numerical results for models in which sudden column removal is considered (*i.e.* with strong inertial and dynamic effects), permitting a closer investigation of the structural dynamic behavior and potential strain rate effects;

- the updating of the structure mass matrix as a function of structural deformation, for better representation of the physical structure;

- the modelling of other failure scenarios, including removal of internal columns and/or columns located on different floors;

- the modelling of different initial failure events in order to simulate dynamic loads as the impact of vehicles and the explosion of a bomb;

67

- the association of plasticity and damage (elastic stiffness degradation) in the representation of the constitutive material behavior;

- the extension of the formulation to three dimensional models which would allow for the inclusion of the resistance introduced by the concrete slabs and also by the out-of-plane beams;

- the inclusion of shear and torsional effects in a 3D scenario and the modelling of failure along the three axes, aimed at a more complete understanding of the phenomenon;

- the parallel implementation of the code for larger structures in order to overcome the higher computational cost implied in three-dimensional modelling.

Bibliography

[1] MARJANISHVILI, S. M. "Progressive analysis procedure for progressive collapse", *Journal of Performance of Constructed Facilities*, v. 18, n. 2, pp. 79–85, 2004.

[2] MASOERO, E., WITTEL, F. K., HERRMANN, H. J., et al. "Progressive collapse mechanisms of brittle and ductile framed structures", *Journal of Engineering Mechanics*, v. 136, n. 8, pp. 987–995, 2010.

[3] PEARSON, C., DELATTE, N. "Ronan Point Apartment tower collapse and its effect on building codes", *Journal of Performance of Constructed Facilities*, v. 19, n. 2, pp. 172–177, 2005.

[4] . http://en.wikipedia.org/wiki/File:Ronan_Point_-_Daily_Telegraph.jpg (Last acess: 12/09/2014).

[5] VLASSIS, A. G. *Progressive collapse assessment of tall buildings*. Ph.D. thesis, Imperial College London, London, United Kingdom, 2007.

[6] MITAL, A., DESAI, A., SUBRAMANIAN, A. *Product Development: a structured approach to consumer product development, design, and manufacture*. 1 ed. United Kingdom, Butterworth-Heineman, 2008.

[7] . https://www.oklahomacitynationalmemorial.org/uploads/documents/Construction%20Elements1.pdf (Last acess: 12/09/2014).

[8] NPS. "*Oklahoma City National Memorial*". National Park Service, 2011. http://www.nps.gov/okci/faqs.htm (Last acess: 12/09/2014).

[9] HOFFMAN, D. "*The cost of terror: Oklahoma City bombing cost $681 million plus lives*". 2010. http://wallstcheatsheet.com/business/economy/the-cost-of-terror-oklahoma-city-bombing-cost-681-million-plus-lives.html/ (Last acess: 12/09/2014).

[10] . http://www.petervintonjr.com/commentary/murrahbldg.jpg
(Last acess: 12/09/2014).

[11] GSA. "*GSA security criteria - draft revision*". United States General Services
Administration, Washington - D.C.,USA, 1997.

[12] NADEL, B. A. "*Designing for Security*". 1998. http://archrecord.construction.
com/resources/conteduc/archives/research/3_98_1.asp
(Last acess: 12/09/2014).

[13] FEMA. "*World Trade Center building performance study: data collection, pre-
liminary observations, and recommendations*". Federal Emergency Man-
agement Agency, Washington - D.C.,USA, 2002.

[14] . https://encrypted-tbn0.gstatic.com/images?q=tbn:ANd9GcQ4471EV71G4aVt
xsq2lrUdiv1Nw9lQbOiDMZEvO8iCi3HKzioD7bNnLQ
(Last access: 12/09/2014).

[15] . http://media.cleveland.com/science_impact/photo/south-wtc-collapse-by-ap
-amy-sancettajpg-f175d8e6007bc184.jpg
(Last access: 12/09/2014).

[16] . http://cdn.rsvlts.com/wp-content/uploads/2012/09/s_a29_90105585-930x8
01.jpeg
(Last access: 12/09/2014).

[17] COPPOLA, D., HARRALD, J. R., YELETAYSI, S. "Assessing the financial
impacts of the World Trade Center attacks on publicy held corporations".
Proceedings, 10th Annual Tiems Conference, Provance, France, 2003.

[18] NIST. "*Final report on the collapse of the World Trade Center towers*". National
Institute of Standards and Technology. US Department of Commerce,
Washington - D.C.,USA, 2005.

[19] FACILITIESNET. "*ICC approves new code changes based on recommendations
from NIST World Trade Center investigation*". 2008.
http://www.facilitiesnet.com/designconstruction/article/ICC-Approves-
New-Code-Changes-Based-on-Recommendations-from-NIST-World-
Trade-Center-Investigation-9850 (Last acess: 12/09/2014).

[20] LIMA, M. "*Perícia conclui que erro no cálculo estrutural causou desabamento
de edifício em Belém*". 2011. http://piniweb.pini.com.br/construcao/tecn
ologia-materiais/pericia-conclui-que-erro-no-calculo-estrutural-causou-
desabamento-de-213840-1.aspx (Last acess: 12/09/2014).

[21] COURI, G. A., DEUTSCH, S. F. "Ruína do Ed. Liberdade - Cinelândia". *XVII COBREAP - Congresso Brasileiro de Engenharia de Avaliações e Perícias - IBAPE*, Santa Catarina, Brazil, 2013.

[22] . https://encrypted-tbn2.gstatic.com/images?q=tbn:ANd9GcQpr-KftX5avN9a mDfiGxacqKW0vHRzN_oHITxtk-PlgU_3_3Z1vw
(Last access: 12/09/2014).

[23] . http://s2.glbimg.com/FTr7liPAdlnJMByCyAnehr7L7Q2EtNtD8AArbgVh3J NH6Amnwb99YkZJ85BFtNZS/s.glbimg.com/jo/g1/f/original/2012/01 /29/predio_compara.jpg
(Last access: 12/09/2014).

[24] GARCIA, G. "Depois de cinquenta anos da tragédia, Comurba ainda é mistério em Piracicaba". 2014. http://www.jornaldepiracicaba.com.br/capa/defaul t.asp?p=viewnot&cat=viewnot&idnot=222891
(Last access: 12/09/2014).

[25] . http://1.bp.blogspot.com/_D1tuttPr5SY/TLNIckqdRgI/AAAAAAAAAk/ sbEGk4YF6Ds/s320/0538.jpg
(Last access: 12/09/2014).

[26] . http://www.aprovincia.com.br/wp-content/uploads/2012/08/a4c37707a927 aa4748c761b71b3288f4.jpg
(Last access: 12/09/2014).

[27] OLIVEIRA, H. S. "Decisões: Sentença do caso Sérgio Augusto Naya (Edifícios Palace I e II /RJ)". 2001. http://bsolucoes.com.br/projetos/novositeibccri m/artigo/389-Decisoes:-Sentenca-do-caso-Sergio-Augusto-Naya-%28Edifi cios-Palace-I-e-II–RJ%29..
(Last access: 12/09/2014).

[28] . http://www.revistadehistoria.com.br/uploads/docs/images/images/Palace_II
(Last access: 12/09/2014).

[29] GLOBO. "Desabamento de prédio no Recife causa preocupação na cidade." 2014. http://g1.globo.com/jornal-nacional/noticia/2014/08/desabament o-de-predio-no-recife-causa-preocupacao-na-cidade.html
(Last access: 12/09/2014).

[30] MELO, J. A. C. *Análise de Laudos Emitidos sobre "Prédios Tipo Caixão" da Região Metropolitana de Recife: Causas Apontadas para os Desabamentos e Interdições*. Masters dissertation, Universidade Católica de Pernambuco, Recife, Pernambuco, Brazil, 2007.

[31] MATOS, G. http://noticias.ne10.uol.com.br/grande-recife/noticia/2014/08/01 /parte-de-predio-desaba-na-zona-sul-do-recife-501795.php (Last access: 12/09/2014).

[32] LEW, H. S., BAO, Y., SADEK, F., et al. "An experimental and computational study of reinforced concrete assemblies under a column removal scenario". National Institute of Standards and Technology. US Department of Commerce.

[33] YI, W. J., HE, Q. F., XIAO, Y., et al. "Experimental study on progressive collapse-resistant behavior of reinforced concrete frame structures", *ACI Structural Journal*, v. 105, n. 4, pp. 433–440, 2008.

[34] CRISFIELD, M. A. *Non-linear finite element analysis of solids and structures*, v. I. Chichester, John Wiley & Sons, 1997. 211-219.

[35] BATTINI, J.-M. *Corotational beam elements in instability problems*. PhD, Royal Institute of Technology, Stockholm, Sweden, 2002.

[36] IRIBARREN, B. S., BERKE, P., BOUILLARD, P., et al. "Investigation of the influence of design and material parameters in the progressive collapse analysis of RC structures", *Engineering Structures*, v. 33, n. 10, pp. 2805– 2820, 2011.

[37] CEN. "*EN 1992: Eurocode 2 - design of concrete structures* ". Comité Européen de Normalisation, Brussels, Belgium, 2004.

[38] *fib*. "*fib* Bulletin 42: Constitutive modelling of high strength/high performance concrete". International Federation for Structural Concrete (*fib*), Lausanne, Switzerland, 2008. state-of-art report.

[39] *fib*. "*fib* Bulletin 45: Practitioners' guide to finite element modelling of reinforced concrete structures". International Federation for Structural Concrete (*fib*), Lausanne, Switzerland, 2008. state-of-art report.

[40] ABNT. "*NBR 6118: projeto de estruturas de concreto: procedimento*". Associação Brasileira de Normas Técnicas, Rio de Janeiro, Brasil, 2003.

[41] GOUVERNEUR, D., CASPEELE, R., TAERWE, L. "Experimental investigation of the load-displacement behaviour under catenary action in a restrained reinforced concrete slab strip", *Engineering Structures*, v. 49, n. 4, pp. 1007–1016, 2013.

[42] SASANI, M., BAZAN, M., SAGIROGLU, S. "Experimental and analytical progressive collapse evaluation of actual reinforced concrete structure", *ACI Structural Journal*, v. 104, n. 6, pp. 731–739, 2007.

[43] SASANI, M., KAZEMI, A., SAGIROGLU, S., et al. "Progressive Collapse Resistance of an Actual 11-Story Structure Subjected to Severe Initial Damage", *Journal of Structural Engineering*, v. 137, n. 9, pp. 893–902, 2011.

[44] KOKOT, S., ANTHOINE, A., NEGRO, P., et al. "Static and dynamic analysis of a reinforced concrete flat slab frame building for progressive collapse". N. JRC 62663, European Commission, Joint Research Centre, 2010.

[45] QIAN, K., LI, B. "Slab effects on response of reinforced concrete substructures after loss of corner column", *ACI Structural Journal*, v. 109, n. 6, pp. 845–856, 2012.

[46] SADEK, F., MAIN, J. A., LEW, H. S., et al. "Testing and analysis of steel and concrete beam-column assemblies under a column removal scenario", *Journal of Structural Engineering*, v. 137, n. 9, pp. 881–892, 2011.

[47] SU, Y., TIAN, Y., SONG, X. "Progressive collapse resistance of axially-restrained frame beams", *ACI Structural Journal*, v. 106, n. 5, pp. 600–607, 2009.

[48] SASANI, M., KROPELNICKI, J. "Progressive collapse analysis of an RC structure", *The Structural Design of Tall and Special Buildings*, v. 17, n. 4, pp. 757–771, 2008.

[49] LASKAR, A., GU, H., MO, Y. L., et al. "Progressive collapse of a two-story reinforced concrete frame with embedded smart aggregates", *Smart Materials and Structures*, v. 18, n. 7, pp. 1–10, 2009.

[50] YU, J., TAN, K. "Experimental and numerical investigation on progressive collapse resistance of reinforced concrete beam column sub-assemblages", *Engineering Structures*, v. 55, n. 10, pp. 90–106, 2013.

[51] FARHANGVESALI, N., VALIPOUR, H., SAMALI, B., et al. "Development of arching action in longitudinally-restrained reinforced concrete beams", *Construction and Building Materials*, v. 47, n. 10, pp. 7–19, 2013.

[52] KO, Y.-F., PHUNG, C. "Nonlinear static cyclic pushover analysis for flexural failure of reinforced concrete bridge columns with combined damage mechanisms", *Acta Mechanica*, v. 225, pp. 477–492, 2014.

[53] SPACONE, E., FILIPPOU, F. C., TAUCER, F. F. "Fibre beam-column model for non-linear analysis of R/C frames: Part I. Formulation", *Earthquake Engineering & Structural Dynamics*, v. 25, n. 7, pp. 711–725, 1996.

[54] SPACONE, E., FILIPPOU, F. C., TAUCER, F. F. "Fibre beam-column model for non-linear analysis of R/C frames: Part II. Applications", *Earthquake Engineering & Structural Dynamics*, v. 25, n. 7, pp. 727–742, 1996.

[55] PETRANGELI, M., PINTO, P. E., CIAMPI, V. "Fiber Element for Cyclic Bending and Shear of RC Structures. I: Theory", *Journal of Engineering Mechanics*, v. 125, n. 9, pp. 994–1001, 1999.

[56] PETRANGELI, M. "Fiber Element for Cyclic Bending and Shear of RC Structures. II: Verification", *Journal of Engineering Mechanics*, v. 125, n. 9, pp. 1002–1009, 1999.

[57] BIAN, Z., HU, S.-M., MARTIN, R. "Comparing Small Visual Differences between Conforming Meshes". In: Chen, F., J (Eds.), *Advances in Geometric Modeling and Processing*, Springer Berlin Heidelberg.

[58] MAZARS, J., KOTRONIS, P., RAGUENEAU, F., et al. "Using multifiber beams to account for shear and torsion: Applications to concrete structural elements", *Computer Methods in Applied Mechanics and Engineering*, v. 195, n. 52, pp. 7264–7281, 2006.

[59] BACINSKAS, D., KAKLAUSKAS, G., GRIBNIAK, V., et al. "Layer model for long-term deflection analysis of cracked reinforced concrete bending members", *Mechanics of Time-Dependent Materials*, v. 16, n. 2, pp. 117–127, 2012.

[60] STRAMANDINOLI, R. S. B., LA ROVERE, H. L. "FE model for nonlinear analysis of reinforced concrete beams considering shear deformation", *Engineering Structures*, v. 35, pp. 244–253, 2012.

[61] BENTZ, E. C., VECCHIO, F. J., COLLINS, M. P. "Simplified Modified Compression Field Theory for Calculating Shear Strength of Reinforced Concrete Elements", *ACI Structural Journal*, v. 103, n. 4, pp. 614–624, 2006.

[62] KOKOT, S., ANTHOINE, A., NEGRO, P., et al. "Static and dynamic analysis of a reinforced concrete flat slab frame building for progressive collapse", *Engineering Structures*, v. 40, pp. 205–217, 2012.

[63] IRIBARREN, B. S. *Progressive collapse simulation of reinforced concrete structures: Influence of design and material parameters and investigation of*

the strain rate effects. PhD thesis, Université Libre de Bruxelles (Faculty of Applied Sciences) and the Royal Military Academy (Polytechnical Faculty), Brussels, Belgium, 2011.

[64] BAO, Y., KUNNATH, S. K., EL-TAWIL, S., et al. "Macromodel-Based Simulation of Progressive Collapse: RC Frame Structures", *Journal of Structural Engineering*, v. 134, n. 7, pp. 1079–1091, 2008.

[65] DAT, P. X., HAI, T. K. "Membrane actions of RC slabs in mitigating progressive collapse of building structures", *Engineering Structures*, v. (2011 - In Press, Corrected Proof), 2011.

[66] ELKOLY, S., EL-ARISS, B. "Progressive collapse evaluation of externally mitigated reinforced concrete beams", *Engineering Failure Analysis*, v. 40, n. 5, pp. 33–47, 2014.

[67] KEYVANI, L., SASANI, M., MIRZAEI, Y. "Compressive membrane action in progressive collapse resistance of RC flat plates", *Engineering Structures*, v. 59, n. 2, pp. 554–56, 2014.

[68] XU, J., LIU, X. "A two-step approach to progressive collapse analysis of building structures under blast loading", *Journal of Shanghai Jiaotong University (Science)*, v. 135, n. 4, pp. 393–397, 2009.

[69] ACI. "Building Code Requirements for Structural Concrete and Commentary (ACI 318m-05)". American Concrete Institute, Farmington Hills, USA, 2005.

[70] ASCE. "*Minimum Design Loads for Buildings and Other Structures*". American Society of Civil Engineers, Reston, Virginia, USA, 2010.

[71] DOD. "Unified Facilities Criteria UFC 4-023-03: Design of buildings to resist progressive collapse". Department of Defense (DoD), USA, 2013.

[72] DOD. "Unified Facilities Criteria UFC 3-301-01: Structural Engineering". Department of Defense (DoD), USA, 2014.

[73] GSA. "Progressive collapse analysis and design guidelines for new federal office Buildings and Major Modernization Project". GSA - United States General Services Administration, Washington - D.C.,USA, 2003.

[74] GSA. "Alternate Path Analysis and Design Guidelines for Progressive Collapse Resistance". GSA - United States General Services Administration, Washington - D.C.,USA, 2013.

[75] ISC. "The Risk Management Process for Federal Facilities: An Interagency Security Committee Standard". Interagency Security Committee, Washington - D.C.,USA, 2013.

[76] GSA. "Facility Security Requirements for Explosive Devices Applicable to Facility Security Levels III and IV". GSA - United States General Services Administration, Washington - D.C.,USA, 2011.

[77] ABNT. "*NBR 9062: projeto e execução de estruturas de concreto pré-moldado*". Associação Brasileira de Normas Técnicas, Rio de Janeiro, Brasil, 2006.

[78] CEN. "*EN 1991: Eurocode 1 - actions on structures* ". Comité Européen de Normalisation, Brussels, Belgium, 2002-2006.

[79] HM-GOVERNEMENT. "The building regulations 2010 - Structure". RIBA Bookshops, London, United Kingdom, 2013.

[80] HUSEM, M., PUL, S. "Investigation of stress-strain models for confined high strength concrete", *Sãdhanã*, v. 32, n. 3, pp. 243–252, 2007.

[81] MANDER, J. B., PRIESTLEY, M. J. N., PARK, R. "Observed stress-strain behavior of confined concrete", *Journal of Structural Engineering*, v. 114, n. 8, pp. 1827–1849, 1988.

[82] SAATCIOGLU, M., GRIRA, M. "Confinement of reinforced concrete columns with welded reinforcement grids", *ACI Structural Journal*, v. 96, n. 1, pp. 29–39, 1999.

[83] HO, J. C. M., LAM, J. Y. K., KWAN, A. K. H. "Effectiveness of adding confinement for ductility improvement of high-strength concrete columns", *Engineering Structures*, v. 32, n. 3, pp. 714–725, 2010.

[84] BHOWMICK, R., SHARMA, U., BHARGAVA, P. "Numerical simulation of confined concrete columns and a parametric study", *Asian Journal of Civil Engineering (Buiding and Housing)*, v. 7, n. 3, pp. 269–286, 2006.

[85] BISCHOFF, P. H., PERRY, S. H. "Compressive behaviour of concrete at high strain rates", *Materials and Structures*, v. 24, n. 6, pp. 425–450, 1991.

[86] MALVAR, L. J., CRAWFORD, J. E. "Dynamic increase factors for concrete". Twenty-Eighth DDESB Seminar, Orlando - FL,USA, 1998.

[87] HEERES, O. M., SUIKER, A. S. J., BORST, R. "A comparison between the Perzyna viscoplastic model and the Consistency viscoplastic model", *European Journal of Mechanics - A/Solids*, v. 21, n. 1, pp. 1–12, 2002.

[88] "ACI 318-08: Building Code Requirements for Structural Concrete". American Concrete Institute, USA, 2007.

[89] MANDER, J. B., PRIESTLEY, M. J. N., PARK, R. "Theoretical Stress-Strain Model for Confined Concrete", *Journal of Structural Engineering*, v. 114, n. 8, pp. 1804–1825, 1988.

[90] SRI RAVINDRARAJAH, R. "Casting delay on workability and strength of concrete", *The International Journal of Cement Composites and Lightweight Concrete*, v. 7, n. 2, pp. 109–113, 1985.

[91] SCOTT, B. D., PARK, R., PRIESTLEY, M. J. N. "Stress-strain behaviour of concrete confined by overlapping hoops at low and high strain rates", *ACI Journal*, v. 79, n. 1, pp. 13–27, 1982.

[92] TOOSSI, M. "Variation of concrete strength due to pressure exerted on fresh concrete", *Cement and Concrete Research*, v. 10, n. 6, pp. 845–852, 1980.

[93] RANJBAR, M. M., HOSSEINALI BEYGI, M., NIKBIN, I. M., et al. "Evaluation of the Strength Variation of Normal and Lightweight Self-Compacting Concrete in Full Scale Walls", *Materials Technology*, v. 45, n. 6, pp. 571–577, 2011.

[94] BOURNONVILLE, M., DAHNKE, J., DARWIN, D. "Statistical analysis of the mechanical properties and weight of reinforcing bars". N. 04-1, The University of Kansas Structural Engineering and Materials Laboratory, 2004.

[95] "GB50010: Code for Design of Concrete Structures". House of Building Industry, China, 2002.

[96] LIANQING, S., FENGZHEN, W., MING, L., et al. "Research and development on HRB400 Reinforced Bars in Handan Steel". International Symposium 2003 on the Research and Application of High Strength Reinforcing Bar, Hangzhou, China, 2003.

[97] BUILDSOFT NV. Diamonds 2010 r.01. http://www.buildsoft.eu (Last access: 07/03/2013).

[98] CYPE. "Cypecad 2011". http://www.cype.pt/ (Last access: 07/03/2013).

[99] LEE, Y. H., SCANLON, A. "Comparison of One- and Two-Way Slab Minimum Thickness Provisions in Building Codes and Standards", *ACI Structural Journal*, v. 102, n. 2, pp. 157–163, 2010.

[100] ABNT. "*NBR 7480: aço destinado a armaduras para estruturas de concreto armado - Especificação*". Associação Brasileira de Normas Técnicas, Rio de Janeiro, Brasil, 2008.

[101] SMITH, P. D., HETHERINGTON, J. G. *Blast and Ballistic Loading of Structures*. 1 ed. Boca Raton, FL, USA, CRC Press, 1994.

Appendix A

Related Publications

The following publications are products of this research.

A.1   Congress Papers

- Sousa, J. B. M.; Oliveira, C. E. M.; Silveira, R. A. da M., *Eventos envolvendo colapso progressivo e suas implicaçoẽs*, XXXII CILAMCE - Iberian Latin-American Congress on Computational Methods in Engineering, 2011, Ouro Preto.

- Oliveira, C. E. M.; Silveira, R. A. da M.; Sousa, J. B. M., *Meétodos e parâmetros da análise do colapso progressivo de edifícios*, XXXII CILAMCE - Iberian Latin-American Congress on Computational Methods in Engineering, 2011, Ouro Preto.

- Oliveira, C. E. M.; Berke, P. Z.; Silveira, R. A. M.; Massart, T. J., *Computational assessment of the progressive collapse of a five storey structure considering two different building codes*, 4th International Conference on Computational Methods in Structural Dynamics and Earth Engineering, 2013, Kos.

- Oliveira, C. E. M.; Marchis, A.; Berke, P. Z.; Silveira, R. A. M.; Massart, T. J., *Computational analysis of a reinforced concrete planar frame using corotational multilayered beam finite elements, correlated to experimental results*, XXXIV CILAMCE - Iberian Latin-American Congress on Computational Methods in Engineering, 2013, Pirenópolis.

A.2   Journal Papers

- Oliveira, C. E. M.; Batelo, E. A. P.; Berke, P. Z.; Silveira, R. A. M.; Massart, T. J., *Nonlinear analysis of the progressive collapse of reinforced concrete plane frames using a multilayered beam formulation*, IBRACON Structures and Materials Journal, 2014.

- Oliveira, C. E. M.; Marchis, A.; Berke, P. Z.; Silveira, R. A. M.; Massart, T. J., *Computational Investigation of experimentally collapsed reinforced concrete structures using a nonlinear multilayered beam formulation*, (to be submitted).

Appendix B

Algorithms

B.1   Dynamic Solution algorithm

```
PROCESSING OF MODEL DATA
**************************************************************************
```

1. Structure model data
2. Load model data
3. Allocate arrays (vector of displacements, vector of displacement resi-
   duals, vector of external forces, vector of internal forces, vector of
   nodal velocities, vector of nodal accelerations)
4. Initialize arrays
5. Initialize deformation history
6. Compute parameters for Newmark time integration scheme
7. Get previous results (if restarting analysis)
8. Initialize the constant mass matrix for the dynamic problem

```
INCREMENTAL PROCEDURE
**************************************************************************
```

9. While the number of increments is lower than the maximum number of
   increments:
   - a. Update number of increments
   - b. Read load factor and time
   - c. Perform Newmark prediction of nodal displacements, nodal veloc-
     ities and nodal accelerations
   - d. Compute the vector of residual forces

e. Start the iteration loop

----

      eI. While the residual is higher than the tolerance and the
          number of iterations is lower than the maximum number of
          iterations:

     eII. Compute structural stiffness matrix

   eIII. Update the external force vector as a function of the
          vector of residual displacements

    eIV. Construct new iterative solution using Newmark update
          formula

      eV. Compute new internal nodal forces

    eVI. Check convergence of the internal force vector

   eVII. Compute new vector of residual forces

----

f. If convergence was achieved:

----

      fI. Update the vector of nodal displacements, velocities
          and accelerations

     fII. Process deformation history

   fIII. Save reaction forces vs. displacement

    fIV. Generate output

     fV. Generate fibers' output

----

g. If the increment failed to converge, refine load step

B.2   Internal force vector algorithm

```
ELEMENT LEVEL
***********************************************************************
```

1. Load element data (number of fiber data, number of layers, number of
   integration point data, number of integration points, number of element
   data, shape function, number of element degrees of freedom, number of
   nodes, number of nodal degrees of freedom, etc.)
2. Compute previous and current nodal coordinates
3. Compute previous and current lengths
4. Compute alpha and beta
5. Compute local displacements
6. Compute transformation matrix **T** and auxiliary vectors **r** and **z**
7. Compute the local coordinates (xi) and weight factors (wi) associated
   to the integration points
8. For each integration point (i)

```
INTEGRATION POINT LEVEL
***********************************************************************
-----------------------------------------------------------------------
```

     a. Compute the matrix of the shape function derivatives – **B**(i)
     b. Compute generalized strains – ε(i) and χ(i)
     c. Read history of the fibers
     d. Compute stress resultants – M(i) and N(i) – and coherent tan-
        gent stiffness matrix – **H**$_c$(i) [1]

```
-----------------------------------------------------------------------
```

9. Compute element stress resultants – M and N (sum of integration point
   parcels)
10. Compute element internal forces

---

[1] The stress resultants are computed from the homogenization of the cross section and involve the computation of normal cross sectional stresses on each fiber. A return mapping procedure is used for both concrete and steel when these materials reach non linear-inelastic levels of stress.

B.3   Stiffness matrix algorithm

ELEMENT LEVEL
```
*************************************************************************
```

1. Load element data (number of fiber data, number of layers, number of
   integration point data, number of integration points, number of element
   data, shape function, number of element degrees of freedom, number of
   nodes, number of nodal degrees of freedom, etc.)
2. Compute previous and current nodal coordinates
3. Compute previous and current lengths
4. Compute alpha and beta
5. Compute local displacements
6. Compute transformation matrix $\mathbf{T}$ and auxiliary vectors $\mathbf{r}$ and $\mathbf{z}$
7. Compute the local coordinates (x_i) and weight factors(w_i) associated to
   the integration points
8. For each integration point (i)

INTEGRATION POINT LEVEL
```
*************************************************************************
-------------------------------------------------------------------------
```
     a. Read coherent tangent stiffness matrix from history - $\mathbf{H_c}$(i)

     b. Compute the matrix of the shape function derivatives - $\mathbf{B}$(i)

     c. Compute material stiffness matrix - $\mathbf{K_m}$(i)
```
-------------------------------------------------------------------------
```

9. Compute element material stiffness matrix - $\mathbf{K_M}$
10. Read element stress resultants (N and M)
11. Compute element geometric matrix - $\mathbf{K_G}$
12. Compute element stiffness matrix - $\mathbf{K} = \mathbf{K_M} + \mathbf{K_M}$